ICU patient-on-a-chip emulating orchestration of mast cells and cerebral organoids in neuroinflammation

Check for updates

Pelin Saglam-Metiner [1,7], Sena Yanasik [1,7], Yusuf Caglar Odabasi[1], Jennifer Modamio[2], Moritz Negwer[2], Cigir Biray-Avci[3], Ayse Guler[4], Ali Erturk[2], Ender Yildirim[5,6] & Ozlem Yesil-Celiktas [1,6] ✉

Propofol and midazolam are the current standard of care for prolonged sedation in Intensive Care Units (ICUs). However, the effects and mechanism of these sedatives in brain tissue are unclear. Herein, the development of an ICU patient-on-a-chip platform to elucidate those effects is reported. The humanized neural tissue compartment combines mast cells differentiated from human induced pluripotent stem cells (hiPSCs) with cerebral organoids in a three-dimensional (3D) matrix, which is covered with a membrane populated with human cerebral microvascular endothelial cells (hCMEC/D3) that separates the tissue chamber from the vascular lumen, where sedatives were infused for four days to evaluate neurotoxicity and cell-mediated immune responses. Subsequent to propofol administration, gene expressions of *CD40* and *TNF-α* in mast cells, *AIF1* in microglia and *GFAP/S100B/OLIG2/MBP* in macroglia were elevated, as well as *NOS2*, *CD80, CD40, CD68, IL6* and *TNF-α* mediated proinflammation is noted in cerebral organoids, which resulted in higher expressions of *GJB1, GABA-A* and *NMDAR1* in the tissue construct of the platform. Besides, midazolam administration stimulated expression of *CD40* and *CD203c+* reactivated mast cell proliferation and compromised BBB permeability and decreased TEER values with higher barrier disruption, whereas increased populations of *CD11b+* microglia, higher expressions of *GFAP/DLG4/GJB1* and *GABA-A-/NMDAR1-* identities, as well as glutamate related neurotoxicity and *IL1B, IFNG, IFNA1, IL6* genes mediated proinflammation, resulting in increased apoptotic zones are observed in cerebral organoids. These results suggest that different sedatives cause variations in cell type activation that modulate different pathways related to neuroinflammation and neurotoxicity in the ICU patient-on-chip platform.

Neuroinflammation, a synonym of glial cell reactivity, is a complex cellular response of the immune system to various harmful stimuli in the central nervous system (CNS), which initiates the healing process to protect the brain's cells and overall function[1–3]. In the case of neuroinflammation, the integrity of the blood-brain-barrier (BBB) can also be disrupted by the diffusion of proinflammatory cytokines and inflammatory cells into the brain tissue[4,5]. Inflammatory response facilitates the repairing of damage by eliminating infective agents through innate immune cells such as microglia, mast cells, astrocytes, T-cells and also inflammatory cytokines released from these cells[2,6]. Mast cells communicate with other CNS cells, extracellular

matrix (ECM), and blood vessels, as they are located in the abluminal part (brain side) of the BBB. During development, mast cells circulate in the blood in immature form until they migrate to the brain where they complete their differentiation. Mature mast cells are also capable of migrating from the periphery to the brain. There are important findings supporting that reactivated mast cells disrupt the integrity of the BBB and act as catalysts with the mediators secreted in various circumstances such as stress, inflammation or trauma[3,7]. Moreover, secreted inflammatory mediators, neurotransmitters, and chemo-attractants interact with neurons and microglia through transgranulation, where they can transfer granules to

[1]Department of Bioengineering, Faculty of Engineering, Ege University, Izmir, Türkiye. [2]Institute for Tissue Engineering and Regenerative Medicine (iTERM), Helmholtz Zentrum München, Neuherberg, Germany. [3]Department of Medical Biology, Faculty of Medicine, Ege University, Bornova, Izmir, Türkiye. [4]Department of Neuroscience, Faculty of Medicine, Ege University, Bornova, Izmir, Türkiye. [5]Department of Mechanical Engineering, Middle East Technical University, Ankara, Türkiye. [6]ODTÜ MEMS Center, Ankara, Türkiye. [7]These authors contributed equally: Pelin Saglam-Metiner, Sena Yanasik. ✉e-mail: ozlem.yesil.celiktas@ege.edu.tr

other cells[8,9]. While microglia initiate inflammatory responses, provide repair of the CNS and secrete proinflammatory mediators, they also respond to stimuli produced by degranulation and reactivation of other cells such as mast cells[7]. Indeed, some in vitro studies report direct microglial reactivation occurring as a result of mast cell degranulation[10,11]. Besides the inflammatory response caused by the reactivation of microglia, astrocytes and mast cells has a protective effect, the persistent and prolonged inflammation inhibit neuronal regeneration leading to many neurodegenerative diseases, while the mechanisms still remain unclear[12]. Thus, realistic neuroinflammation outputs should be investigated in advanced preclinical models including both resident immune cells, the BBB structure and brain parenchyma construct[3].

The majority of the recent neuroinflammation studies are based on in vivo rodent models that summarize communication between glia and neurons[13]. However, while the neuronal migration and maturation is observed in around one week in mice, it occurs in an extended time exceeding 20 weeks in human neurogenesis[14]. Furthermore, the human brain has unique anatomical features such as an enlarged external sub-ventricular region containing basal radial glia cells critical for cortical expansion, whereas mice lack this regionalization[15]. Thus, animal models cannot completely mimic the complex and unique structure of human brain physiology due to differences in molecular and cellular composition between species[16,17]. On the other hand, the common in vitro neuroinflammation models elevate co-culturing of human primary, immortalized and/or induced pluripotent stem cells (iPSCs) differentiated CNS cells in 2D manner. But these models lack a complex brain architecture, loss of tissue-specific mechanical properties with cell-cell interactions and can not emulate the complex communication between glial and neuronal cells in a 3D context[18–21]. Within the state-of-the-art technology, easy-to-setup 3D neural tissue models established with iPSCs-induced neural/glial cells, natural brain dECM and brain-on-a-chip platforms have gained importance[2,22,23]. Additionally, 3D unguided, guided and fused brain organoids generated from human iPSCs are utilized as advanced in vitro models that allow the study of realistic brain cellular interactions and structural architecture in recent years[24–27]. These models have significant potential not only for the development of new therapies[28] but also investigation of cellular responses to drug administration at extended durations such as the interventions in ICUs.

Sedatives are frequently used in mechanically ventilated ICU patients. While these drugs provide sedation by slowing down the CNS, the administration time, technique and dosage vary according to the clinical requirement of the patient. For instance, long-term infusion is required, especially for sedated patients with head trauma and status epilepticus[29]. In addition, patients on mechanical ventilation may have infusion periods longer than 48 h[30]. Propofol, a lipid-based agent used in ICU, is administered intravenously to maintain the hypnotic component, while midazolam, one of the most commonly used sedatives, is the most lipophilic benzodiazepine that rapidly crosses the BBB[31,32]. Propofol's good pharmacokinetic properties, such as rapid onset of action and short half-life, make it an important alternative for reducing anxiety and agitation and improving tolerance to mechanical ventilation in critically ill patients admitted to the ICU[33,34]. Propofol and benzodiazepines enhance and prolong GABA binding to the GABA-A receptor located at postsynaptic sites with selective modulation[35]. Recent studies have reported that these GABA agonists may cause neurotoxicity and long-term cognitive problems[36–38], in addition to some studies showing protective effects at lower doses and administration times[39–41]. Besides, most in vitro studies focusing on the effects of sedatives on the CNS, are based on static cultures that lack the mimicry of blood and/or cerebrospinal fluid circulation and 3D human brain physiology[42]. Therefore, the effect and mechanism of these sedative substances in the realistic biomimetic brain tissue model has not been fully elucidated. This study highlighted a newly designed ICU patient-on-a-chip platform that is consisted of a vascular chamber with a membrane lined up hCMEC/D3 to recapitulate the BBB, and a neural tissue formed by co-culturing of hiPSCs differentiated mast cells and cerebral organoids in 3D matrix. We

hypothesize that the administration of propofol and midazolam for specific durations to the on-chip platform allows investigation of the alterations in BBB and the cellular response in neural tissue of ICU patients.

Results

Numerical simulation of velocity and shear stress of ICU patient-on-a-chip platform simplifies determination of operating flow condition

Here, we present an easy to set multi-layered biomimetic microfluidic platform composed of biocompatible polydimethylsiloxane (PDMS) that closely models the BBB and 3D brain parenchyma, by recapitulating the interaction of cerebral organoids and mast cells (Fig. 1a). The BBB was simulated in the presence of shear stress caused by fluid movement in the vascularization layer formed by hCMEC/D3 cells seeded on the poly-ethylene terephthalate (PET) membrane.

First, we conducted simulation studies to ascertain flow conditions preventing cell damage from shear stress while maintaining endothelium physiology. An oscillatory flow motion takes place in 30 sec on the rocker and the flow rate is 18 μL/s at 1 RPM. In the simulations performed under the fluid flow rate condition derived from the specified time, the maximum shear stress was observed to be 6.88×10^{-4} Pa at a maximum velocity of 7.73×10^{-4} m/s (Fig. 1b). We analyzed these values by performing simulation studies under different oscillatory flow conditions (5, 10 RPM) (Supplementary Fig. 1). The maximum shear stress is 2.97×10^{-3} Pa at 5 RPM speed, whereas 7×10^{-3} Pa at 10 RPM speed. Thus, we concluded that the increase in fluid flow rate increased the shear stress on the walls of the vascular layer, where elevated levels would have caused damage to the endothelial cells. In order to provide the ideal physiological conditions for cerebral organoids, we carried out optimization studies using 1 RPM as the flow rate. When the 3D matrix was mimicked, we found the maximum velocity to be 9.4×10^{-4} m/s yielding a maximum shear stress of 0.06×10^{-3} Pa (Fig. 1c), which is ~50- and 116-fold lower than the values obtained for 5 and 10 RPM (2.97×10^{-3}, 6.99×10^{-3} Pa), respectively. As for the tissue construct emulating brain parenchyma, we observed a homogeneous velocity and shear stress distribution in the matrix in which the organoids and mast cells would be embedded. Additionally, we simulated laminar flow conditions to reveal the difference between flow in a 3D matrix and free flow (Supplementary Fig. 1). In the presence of free fluid flow, the maximum velocity on the organoids was 8.04×10^{-4} m/s, leading to an average shear stress of 1.24×10^{-3} Pa. Although the shear stress increased due to porosity in the presence of the 3D matrix, its homogeneous distribution on the organoids showed the importance of the 3D extracellular matrix organization in the platform. We also predicted that the maximum velocity observed in the continuous free flow condition would have resulted in the movement of organoids with the flow, which again reveals the necessity of embedding the organoids in the hydrogel matrix.

iPSC-derived mast cells that are co-cultured with cerebral organoids recapitulate resident immune cells in ICU patient-on-a-chip

We differentiated mast cells from iPSCs in order to understand mast cell-related neural tissue response of an ICU patient to propofol and midazolam administrations. From the first days of the process, we observed mesodermal differentiation from iPSCs to start with changes in desired cell morphology on day 4 after BMP4 treatment. On day 6, immediately after culturing in mast cell (MC) StemPro-1 medium, we observed mesenchymal progenitor floating cells, which we expanded until day 27 with resuspension in MC StemPro-2 medium. From this stage, we cultured the floating cells in monolayer phase with MC monolayer medium for maturation of mast cells, while the progenitor floating cell culture could be continued until day 50 in MC StemPro-2 medium. We continued the proliferative monolayer culture until passage 10, when highly proliferative and specific cell morphologies were maintained (Fig. 2a). We characterized mast cell maturity by measuring expression levels of genes (qRT-PCR) and proteins by western blot (WB) and immunofluorescence staining (IF) (Fig. 2b–d). According to
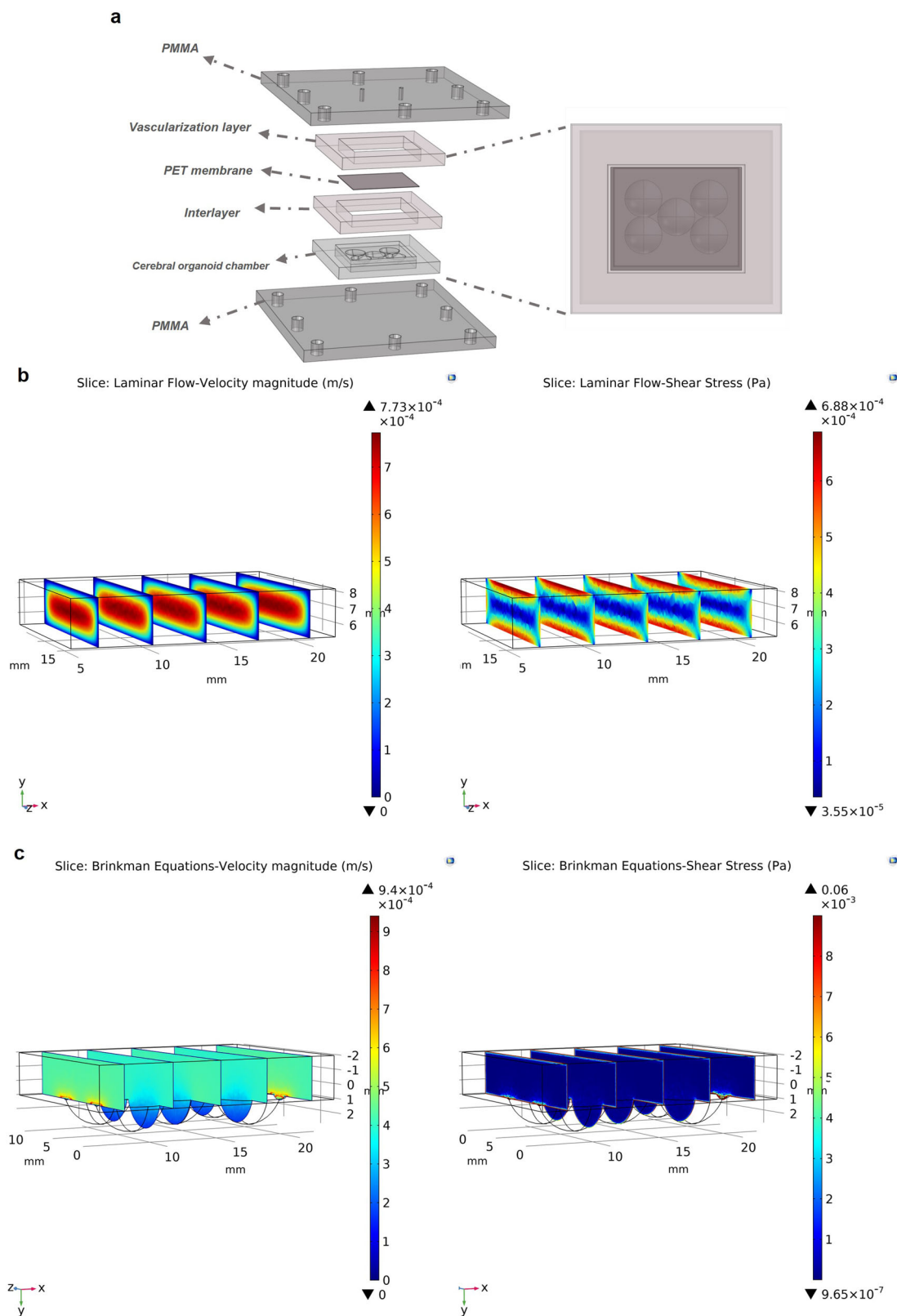
Fig. 1 | Design and simulation of the ICU patient-on-a-chip. a Layer-by-layer view of the ICU patient-on-a-chip platform. **b** numerical simulation of velocity magnitude (m/s) and shear stress (Pa) over BBB at 1 RPM under laminar flow conditions, solved by Navier-stokes equations, and **c** over brain parenchyma at 1 RPM under 3D biomimetic matrix, solved by Brinkman equations.

qRT-PCR results (Fig. 2b, Supplementary Data 1a), both 27 days-old (floating cells) and 45–60 days old (monolayer cells) mast cells lost their stemness identities and gained hematopoietic immune cell character[43], with significantly decreased expression levels of Yamanaka genes (*SOX2,* *POU5F1, KLF4 and MYC*) and significantly increased expression levels of *PTPRC, CD34* and *ITGAM* genes, compared to (undifferentiated) control iPSCs. The increase over time of specific mature mast cell surface antigen gene, c-*KIT*, and high-affinity IgE-receptor specific gene, *FES* (15.4-fold and
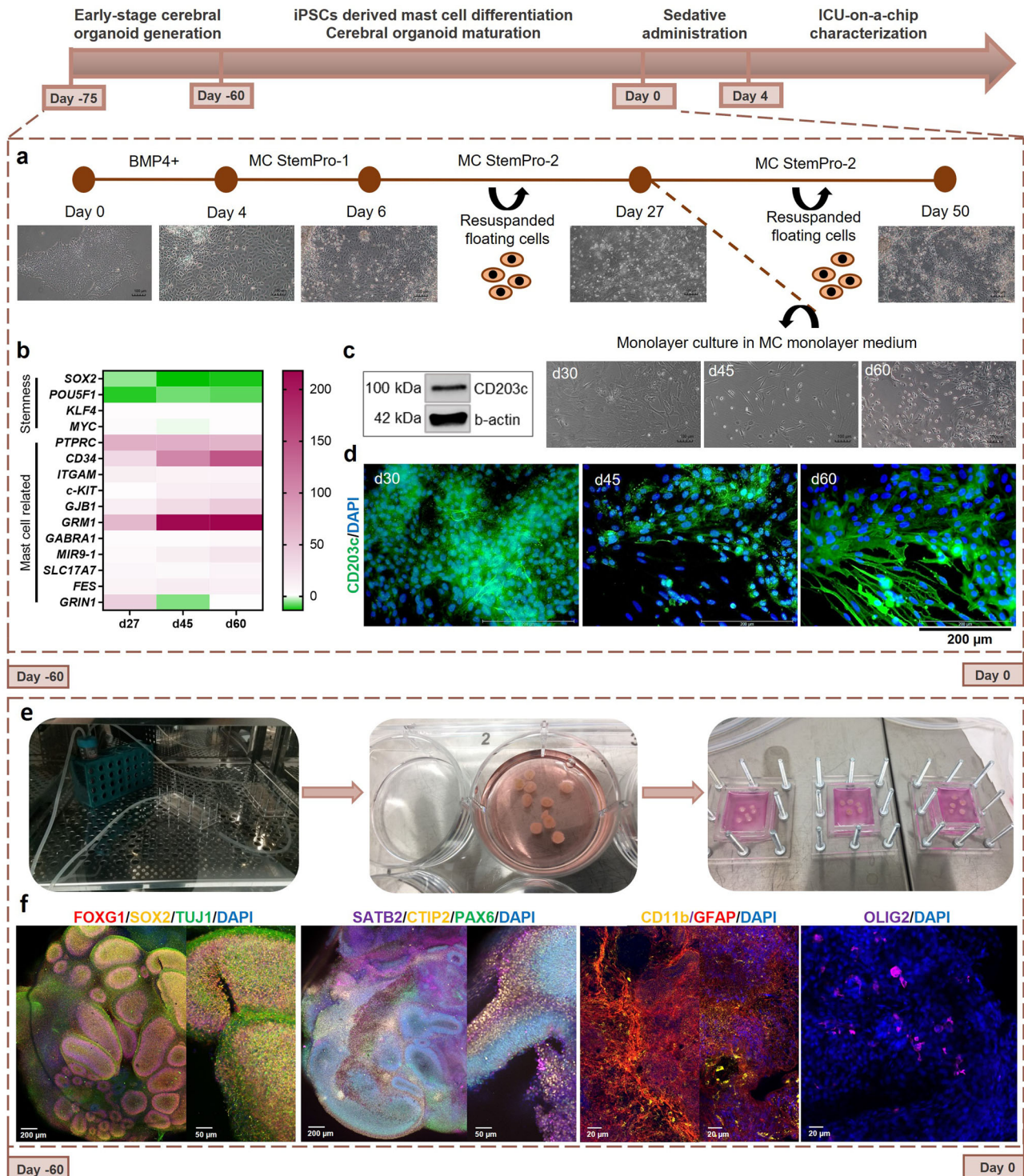
Fig. 2 | Mimicry of neural tissue by co-culturing mast cells and cerebral organoids. a Mast cell differentiation process from iPSCs with brightfield microscopic images (scale bar = 100 μm for ×10 magnification, MOTIC AE31E), b Heatmap generated by qRT-PCR analysis of RNA samples isolated from floating cells on 27 days, and monolayer mast cells on 45 and 60 days compared to control iPSCs (independent repeats = 2) c WB analysis for *CD203c* protein of mature mast cells on day 60 (independent repeats = 2), d IF staining of mast cells on days 30, 45, and 60 of culture with *CD203c* in the mast cell differentiation protocol (scale bars = 200 μm for ×40 magnification images, independent repeats = 3, Zeiss Axio Vert.A1). e Newly designed ICU patient-on-a-chip platform with differentiated mast cells, μ-platform matured cerebral organoids on day 60 and hCMEC/D3 populated membrane, for the BBB evaluation and cellular response in neural tissue recapitulating the response of a patient in the ICU to sedatives. f Brief characterization of μ-platform matured cerebral organoids with whole confocal imaging after tissue clearing, highlighted by *FOXG1, SOX2, TUJ1, SATB2, CTIP2, PAX6, CD11b, GFAP, OLIG2,* and *DAPI* stainings (scale bars = 200 μm for ×5, 50 μm for ×20 and 20 μm for ×40 magnification images, independent replicates = 3, Zeiss LSM 880).

13.2-fold, respectively), also supported the success of the differentiation process. We found three important genes were to increase on day 60 of mast differentiation process: *GRM1*, a metabotropic glutamate receptor specific gene associated with neurodevelopmental disorders[44]. *GJB1*, a junctional transmembrane protein specific gene associated with degranulation of mast cells[45] and *GABRA1*, a specific receptor gene for controlling the majority of inhibitory signaling in the CNS[46], which are related to maturation, reactivation and functionality of mast cells, significantly increased mostly on day 60 as 217.5-fold, 44.5-fold, and 6.2-fold, respectively. We also investigated miRNA expression, as those are key players in differentiation of mature mast cells. We measured an increase in *MIR9-1* gene expression over time (4.5-fold on day 27, 13.7-fold on day 45 and 21.9-fold on day 60), which fits with miRNA upregulation over time during mast cell maturation[47,48]. Additionally, we observed upregulation on day 27 (41-fold) and downregulation on day 45 (6.6-fold) of another ionotropic glutamate receptor subunit specific gene, *GRIN1*, which has been previously described in mast cells in tendon repair[49]. According to WB and IF analyses, a specific cell surface protein of active mast cells, as a type II transmembrane protein, *CD203c*, increased over time throughout the differentiation process mostly on day 60 (Fig. 2c, d). Then, we co-cultured these characterized mast cells with 60 days old μ-platform matured cerebral organoids with *FOXG1+/SOX2+/TUJ1+* forebrain, *SATB2+/CTIP2+/PAX6+* cortical plate and *CD11b+/GFAP+/OLIG2+* micro-macro glial cell identities (see details in our previous study[26]), and completed the ICU patient-on-a-chip by inserting PET membrane seeded with hCMEC/D3 endothelial cells (Fig. 2e, f).

Sedative administration induces BBB permeability via endothelial cell destruction and cellular immune response

In clinical practice, the infusion time of sedative agents may vary according to the patient and their response to treatment. Exposure to propofol for more than 48 h is called prolonged exposure and should not exceed a maximum of 7 days[50]. In order to emulate long-term repetitive sedative exposure in ICU patients (Fig. 3a) in our experimental setup, we first carried out dose-dependent sedative exposures on hCMEC/D3 endothelial cells. Subsequently, we administered the elicited safety doses of 200 μM propofol and 25 μM midazolam in the co-culture media (1:1:1 ratio of endothelial cell, mast cell and cerebral organoid growth media) to the vascular lumen of hydrodynamic platform on days 1 and 2, and then harvested the culture supernatants, BBB layer and neural tissue construct of ICU patient-on-a-chip platform on day 4 for characterization. Specifically, we analyzed identity markers for mediated neuroinflammation associated with mast cells, microglia, macroglia and damaged neurons in neural tissue construct and also BBB layer in ICU platform, in terms of both gene (Supplementary Table 1) and protein expression levels (*CD203c, CD31, ZO-1, vGLUT1, MAP2, CD11b, Ki-67, GABA-A, NMDAR1*) (Fig. 3b). Within this context, we first determined the safety-dose to be administered to the ICU patient-on-a-chip platform. We applied propofol and midazolam (400, 200, 100, 50, 25, 12.5, 6.25, 3.13 μM) to hCMEC/D3 cells for 4 days, observed them day by day under a brightfield microscope (Supplementary Fig. 2), and analyzed cell viabilities quantitatively on day 4 with MTT assay (Supplementary Fig. 3, Supplementary Data 1b). We elicited the safety doses of propofol and midazolam as 200 μM and 25 μM, respectively, since the cell morphologies were observed to be in appropriate shape and structure, whereas cell viabilities were above 70%, with significant differences from the highest doses ($p < 0.0001$ for midazolam and $p < 0.05$ for propofol). At elicited doses, we quantitatively evaluated barrier integrity with FITC permeability test and TEER measurement as gold standards[51].

We found a differential effect on BBB permeability, where 25 μM midazolam administration to the on-chip platform caused significant changes ($p < 0.01$) on BBB permeability with measured FITC value of 4.02×10^{-6} cm/s (see the standard curve in Supplementary Fig. 4a, Supplementary Data 1c). In contrast, 200 μM propofol-administration has not yielded a significant difference in FITC permeability (3.4×10^{-6} cm/s) compared to untreated controls (3.2×10^{-6} cm/s) (Fig. 3c, Supplementary

Data 1d). Similarly, representing the barrier integrity, TEER value of the control group was 421 Ω cm², whereas significant decreases ($p < 0.05$) were noted in both sedative administered groups, mainly for the midazolam group ($p < 0.01$, 146 Ω cm²) (Fig. 3d, Supplementary Data 1e). We also characterized the effect of sedatives on two important endothelial cell-junction complexes, *CD31* and *ZO-1* markers[26]. We found a decrease in viable *CD31*+ endothelial cells after sedative exposure, as well as interruptions to the continuity of *ZO-1* staining mostly subsequent to midazolam administration, which is in line with our increased permeability and decreased TEER values (Fig. 3e).

Midazolam administration stimulates neuroinflammation and neural tissue defect via resident immune cell reactivation

In the neural tissue compartment, we first investigated neuroinflammation-associated activation of mast cells. To this end, we harvested mast cells from ICU patient-on-a-chip platform on day 4 of sedative administration and cultured them on plate, followed by IF staining for *CD203* and cell counting. We found increased *CD203*+ reactivated mast cell population in the midazolam (average of 5.65×10^4 cells/cm², $p < 0.001$) administered group compared to the control (average of 3.52×10^4 cells/cm²), while there was no significant change in numbers of mast cells after propofol (average of 2.73×10^4 cells/cm², $p > 0.05$) administration (Fig. 4a, Supplementary Fig. 5a, Supplementary Data 1f). In addition, we used qRT-PCR to evaluate a wide range of proinflammatory, anti-inflammatory, and specifically mast cell related gene expression levels in harvested cells from the ICU platform (Supplementary Table 1). We found that both sedative administrations resulted in increased expression levels of proinflammatory genes, such as *CD40* (>50-fold), *TNF* (>15-fold) and *NOS2* (>10-fold), and decreased levels of anti-inflammatory genes, most prominently of *IL12B* (>75-fold), *IL13* (>25-fold) and *IL10* (>15-fold). This indicates that sedative administration resulted in a reactivated mast cell-related neuroinflammatory response. While we observed no major changes in non-inflammatory related gene expression levels, *GRIN1* gene levels were significantly decreased in both propofol (53.8-fold) and midazolam (15.8-fold) treated mast cells (Fig. 4b, Supplementary Data 1g). As resident immune cells, cellular sensor and effector in the CNS, microglia and mast cells have been mostly involved in neuroinflammation and neurodegeneration. Under these pathological states, they rapidly release excessive amounts of pathogenic immunomodulatory molecules, such as *TNF-α* and excitatory glutamate[2,52]. Thus, in order to quantify the extent of activated CNS immune cells in the neural tissue compartment following sedative exposure, we measured elevated *TNF-α* and glutamate concentrations as indicators of proinflammation-mediated neuroinflammation from the culture supernatants using ELISA and specific glutamate kit (Fig. 4c, d). We found that *TNF-α* cytokine was released at significantly higher concentrations in both sedative-administered groups ($p < 0.05$) compared to the control group. Interestingly, propofol showed more ($p < 0.01$) proinflammatory effects via *TNF-α* pathway (Fig. 4c, Supplementary Data 1h), which matched our qRPCR results. To investigate the effect of sedatives on immune cell-related glutamate expression, we measured glutamate levels in the culture supernatant with the calorimetric glutamate assay (see the standard curve in Supplementary Fig. 4b, Supplementary Data 1i). In comparison to the control group (24.2 ± 2.4 μM), the groups administered with midazolam (95 ± 4.9 μM, approximately fivefold, $p < 0.001$) and propofol (76 ± 2.4 μM, approximately threefold, $p < 0.01$) exhibited notably elevated releases of glutamate, suggesting the occurrence of neuroinflammation due to the reactivation of immune cells in the CNS (Fig. 4d, Supplementary Data 1j). Finally, in order to understand the changes in the brain parenchyma, we examined cerebral organoids harvested from the neural tissue compartment of the on-chip platform by WST-1 viability assay, qRT-PCR, vDISCO tissue clearing, and TUNEL apoptosis assay (Figs. 4e, g and 5). Although these concentrations of sedatives did not show cytotoxic effects (above 70% cell viability) on monolayer endothelial cells (Supplementary Fig. 3), their cytotoxic effect on cells within the main neural tissue in the ICU patient on-a-chip platform was measured by decreased colorimetric absorbances in
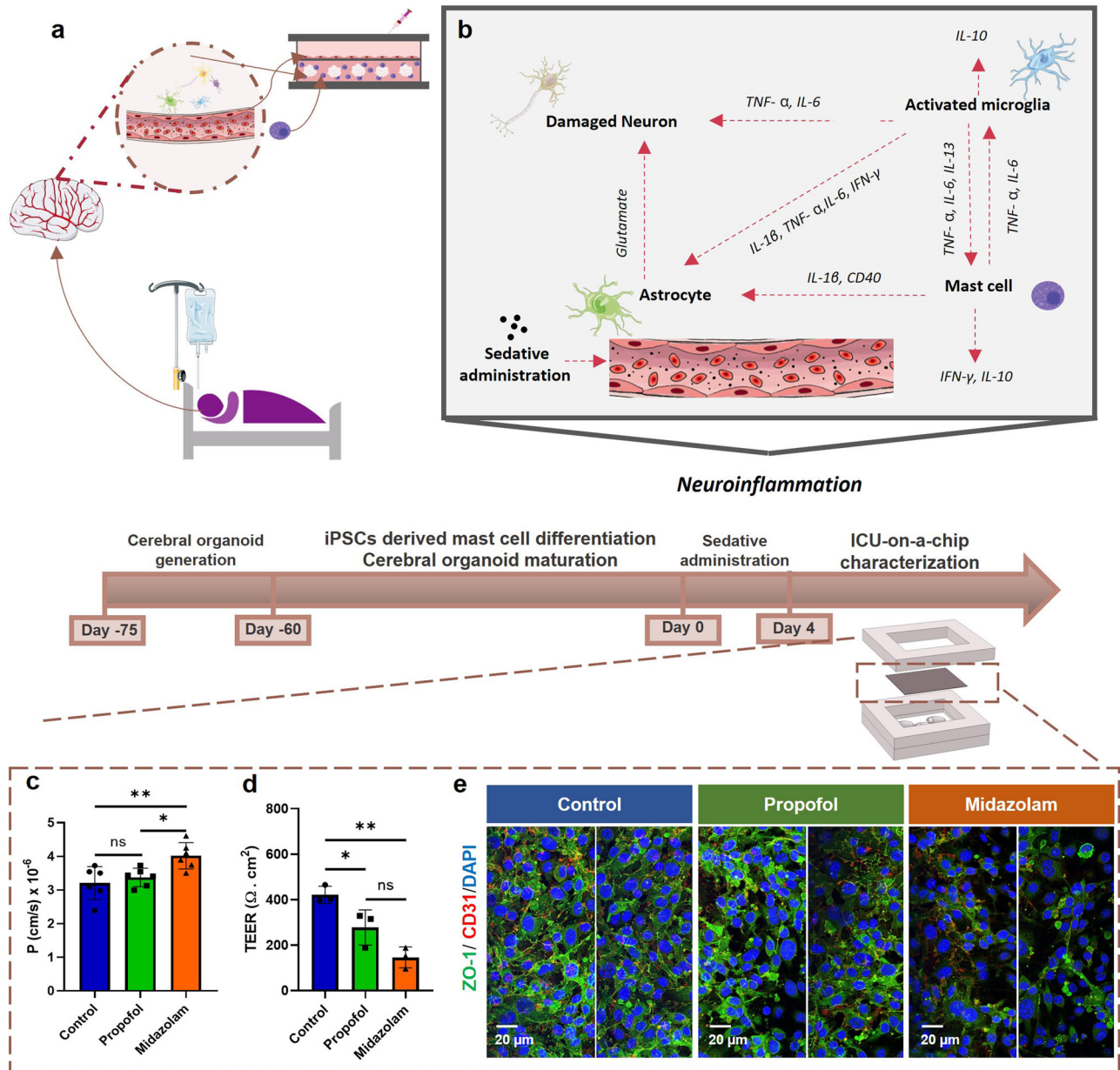
Fig. 3 | Effects on sedative administration permeability and barrier integrity.
a Schematic illustration of sedative administration on ICU patient-on-a-chip platform. **b** recapitulating the interaction between BBB, mast cells, and cerebral organoids inflammatory response by cytokine release from neuronal, glial, and mast cells upon sedative administration; both **a** and **b** are generated with Servier Medical Art, provided by Servier, licensed under a Creative Commons Attribution 3.0 unported license. **c** Fluorescein Isothiocyanate (FITC) permeability assay results of BBB construct at the end of 4 days of sedative administration as P (cm/s × 10^{-6}), and **d** trans-endothelial electrical resistance (TEER) measurement results at the end of 4 days of sedative administration as $\Omega\ cm^2$ (One-way ANOVA Tukey's multiple comparisons test, ns; $p > 0.05$, *$p < 0.05$, **$p < 0.01$, independent replicates = 3). **e** IF staining of *CD31* and *ZO-1* markers (scale bars = 20 μm for ×40 magnification images, independent replicates = 3, Leica Microsystems, Stellaris 5) for BBB construct at the end of 4 days of sedative administration in the ICU patient-on-a-chip.

parallel with cell viabilities, mostly of midazolam ($p < 0.05$), compared to control group (Fig. 4e, Supplementary Data 1k). These findings were also supported by qRT-PCR results where expression levels of the proliferative cell marker *MKI67* gene were significantly decreased in both propofol (12.4-fold) and midazolam (9-fold) administered organoids, and expression levels of the apoptosis marker *CASP3* gene were specifically increased in the midazolam (5.2-fold) group (Fig. 4f, Supplementary Data 1l). As such, we found that propofol led to an increase in the gene expression levels of the macroglia markers *GFAP* (10.4-fold), *S100B* (10.1-fold), *OLIG2* (4.4-fold), *MBP* (4-fold), as well as the microglia marker *AIF1* (6.2-fold). Midazolam-administration resulted in a similar but comparatively lower increase in the gene expression levels of both *GFAP* (7.2-fold) (macroglia) and *ITGAM* (5.7-fold) (microglia). Considering the genes associated with organoid

maturation, we found that propofol-administration led to increases in the expression of *GJB1* (25.3-fold) and *GABRA1* (13.6-fold).

midazolam administration exhibited a similar increase in *GJB1* (7.2-fold) and *DLG4* (12.4-fold) mRNA, but a decrease in the expression levels of *GRIN1* (73.7-fold), *GABRA1* (42-fold), and *GLS* (11-fold). Moreover, we observed increases mostly in the gene expression levels of pro-inflammatory markers *NOS2* (19.2-fold), *CD80* (4.4)-fold, and *CD40* (3.7-fold) in the propofol-administered group. In contrast, with midazolam, we observed increases in *IL1B* (8.3-fold), *IFNG* (4.2-fold), and *IFNA1* (3.3-fold) mRNA levels, which are also indicative of pro-inflammatory expression. With respect to a general pro-inflammatory shift, we observed significant decreases in anti-inflammatory-related gene expression (*IL10, MRC1,* and *STAT6* genes, except *ARG1*) in both sedative groups (Fig. 4f, Supplementary
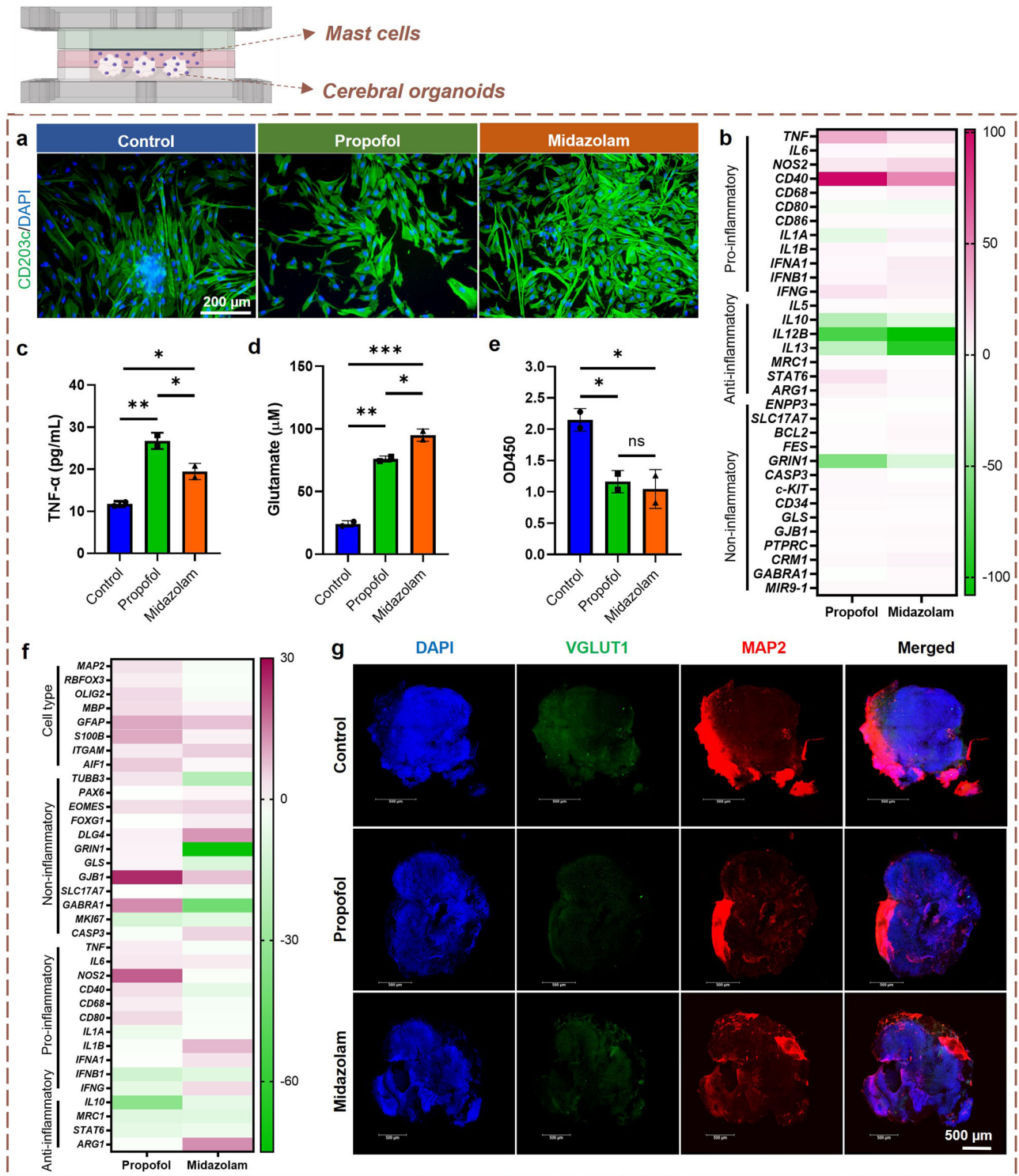
Fig. 4 | Neuroinflammatory and neurotoxic effects of sedative administration on neural tissue. a IF staining of specific mast cell marker *CD203c* (scale bars = 20 μm for ×20 magnification images, independent replicates = 3). **b** Heatmap generated by fold regulation data obtained as a result of qRT-PCR analysis of RNA samples isolated from mast cells (independent repeats = 2). **c** *TNF-α* concentrations (pg/mL) and **d** extracellular glutamate concentrations (μM) in the supernatant, and **e** WST-1 analysis of organoids (one-way ANOVA Tukey's multiple comparisons test, ns;

$p > 0.05$, *$p < 0.05$, **$p < 0.01$, ***$p < 0.001$, independent replicates = 2). **f** Heatmap generated by fold regulation data obtained as a result of qRT-PCR analysis of RNA samples isolated from organoids (independent repeats = 2). **g** 3D confocal microscopy images of *VGLUT1/MAP2* stained vDISCO tissue cleared cerebral organoids harvested from ICU patient-on-a-chip platform at the end of 4 days of sedative administration (scale bar = 500 μm independent replicates = 3, Zeiss LSM 880).

Data 1l). We next wondered whether there would be spatial differences in neuronal markers across the organoids. To this end, we used whole-organoid clearing with the vDISCO protocol and imaged *vGLUT1* and *MAP2*, two neuronal markers for synapses and dendrites[2,26], respectively,

using a confocal microscope (Fig. 4g). Additionally, we performed mean fluorescence intensity analysis using confocal microscopy images to quantitatively corroborate the qualitative data (Supplementary Fig. 5b, Supplementary Data 1m). We observed that the protein expression levels of the
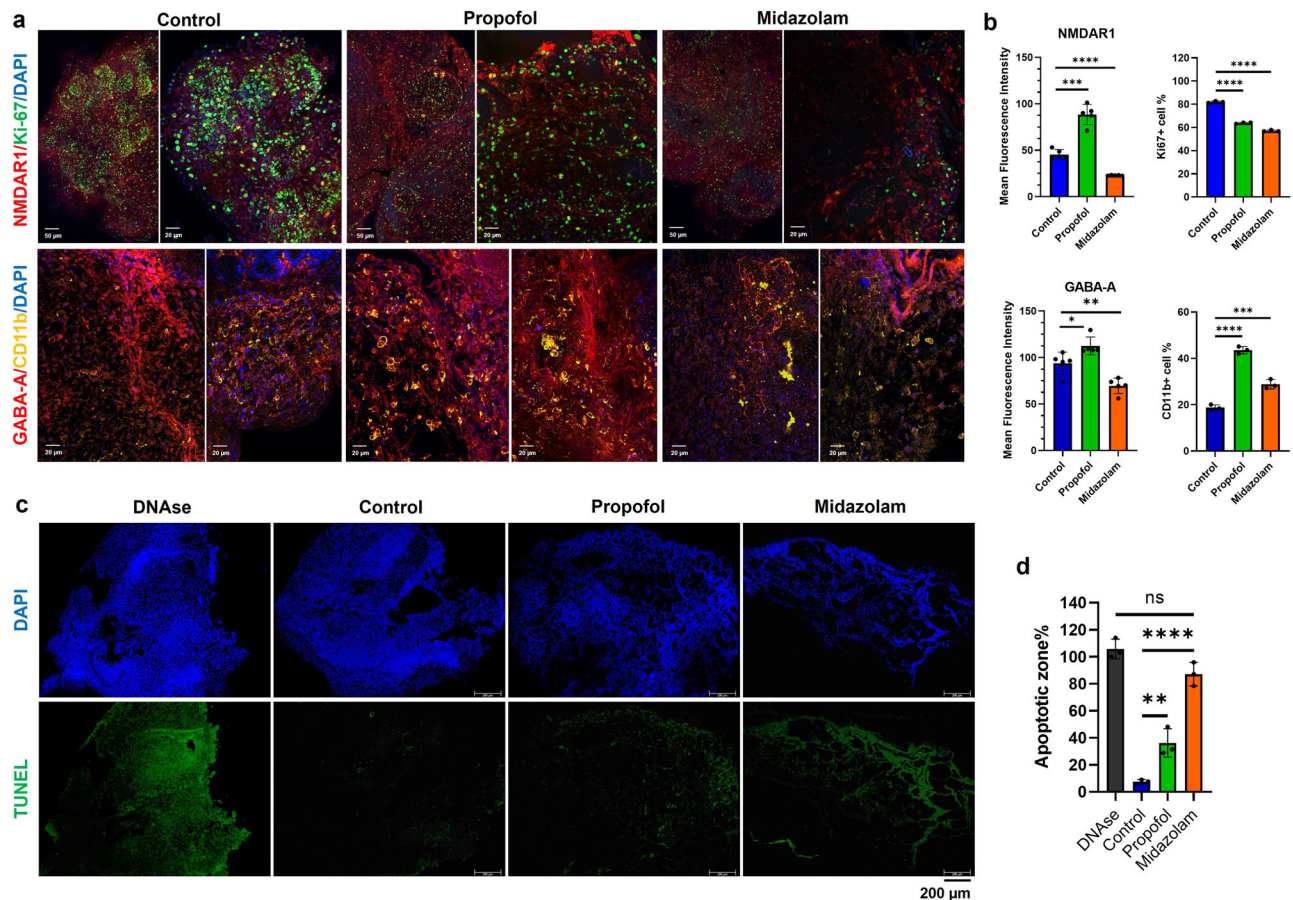
Fig. 5 | Further characterization of neural tissue from ICU patient-on-a-chip platform by IF and TUNEL after sedative administration. a 3D confocal microscopy images of *Ki-67, NMDAR1, GABA-A*, and *CD11b* stained vDISCO tissue cleared cerebral organoids harvested from ICU patient-on-a-chip platform at the end of 4 days of sedative administration (scale bars = 50 μm for ×20 and 20 μm for ×40 magnification images, independent replicates=3, Leica Microsystems, Stellaris 5). **b** Quantification of the mean fluorescence intensity signal of *NMDAR1* and *GABA-A* stainings and *Ki-67* + & *CD11b*+ cell % versus DAPI+ cell countings (One-way ANOVA Tukey's multiple comparisons test, *$p < 0.05$, **$p < 0.01$, ***$p < 0.001$, ****$p < 0.0001$ independent replicates = 3–5). **c** TUNEL apoptosis fluorescent staining images of paraffin sectioned cerebral organoids harvested from ICU patient-on-a-chip platform at the end of 4 days of sedative administration. The DAPI-stained cell nucleus (blue), green fluorescent-stained apoptotic zones in the cell nucleus (green) (scale bar = 200 μm, independent replicates = 3, Zeiss Axio Vert.A1). **d** Percentage of apoptotic zone graph prepared from TUNEL images (independent replicates = 3, one-way ANOVA Tukey's multiple comparisons test, ns; $p > 0.05$, **$p < 0.01$, ****$p < 0.0001$).

presynaptic protein *vGLUT1* were clearly decreased in both sedative-administered groups, mostly in propofol ($p < 0.05$) with a reduced fluorescence intensity of 1.71-fold, compared to the control. Besides, *MAP2*, a marker for dendrites in maturing neurons, was regionally decreased in both sedative administered groups, again mostly in propofol ($p < 0.05$) with a reduced fluorescence intensity of 1.34-fold, compared to the control. It is worth noting that a reduction in the expression of *vGLUT1*, a glutamate transporter located in the membrane of synaptic vesicles in the presynaptic terminal, has been linked to functional impairment following neuroinflammation, neurodegeneration and neuronal damage[26,53–55]. These results support our hypothesis that prolonged administration of propofol and midazolam in ICU patients might cause abnormal CNS immune cell reactivation-mediated neuroinflammation, resulting in neural cell death, BBB disruption and loss of function in neural tissue, due to increased neurotoxic glutamate release.

Additionally, confocal microscopy and quantitative analysis of mean fluorescence intensity and cell counting were performed to examine some of the genes that stood out in the qRT-PCR analysis of cerebral organoids at the protein level (Fig. 5a, b, Supplementary Data 1n). *GABA-A+/CD11b+/Ki-67+/TUNEL−*, which have also been previously characterized in detail at both protein and gene levels[26], were found to exhibit an additionally active *NMDAR1+* cell population with organized tissue structure in the ICU patient-on-a-chip platform. The alterations in the tissue subsequent to

sedative administration was characterized by decreased cellular viability with decreases in *Ki-67* protein expressions ($p < 0.0001$, 18.12% less for propofol, 24.84% less for midazolam), in agreement with qRT-PCR results. While *NMDAR1+* (1.95-fold high, $p < 0.001$) and *GABA-A+* (1.2-fold high, $p < 0.05$) identities clearly increased with highly populated *CD11b+* cells (2.32-fold high, $p < 0.0001$) in the propofol administered group, the increased *CD11b+* cell population (1.53-fold high, $p < 0.001$) was interestingly characterized by decreased *NMDAR1* (regionally, 1.98-fold less, $p < 0.0001$) and *GABA-A* (1.35-fold less, $p < 0.01$) protein expressions after midazolam administration, compared to control group. On the other hand, the TUNEL fluorescent staining was performed to determine apoptotic regions, cell death and cell survival[26] in cerebral organoids harvested from ICU patient-on-a-chip platform after 4 days (Fig. 5c, d, Supplementary Data 1o). DNAse-treated organoid as a positive control displayed DAPI and visible green fluorescence, validating the functionality of the assay. Cell apoptosis was characterized by labeled fragmented DNA breaks in TUNEL + /DAPI+ cells at an apoptotic zone of ~106%. Almost no elevated rates of DNA breakage and cell apoptosis were observed in the organoids of the control group (7.5%), exhibiting more complex cytoarchitecture and regionalization. However, the presence of apoptotic cells in the peripheral regions of the organoids that were administered with sedatives, mostly with midazolam ($p > 0.05$ versus DNAse-treated group), significantly increased (apoptotic zone of 36%, $p < 0.01$, and 87%, $p < 0.0001$, for propofol and

midazolam, respectively) due to neurotoxicity and cell-tissue destructive effects, in parallel with the *Ki-67* and *CASP3* expressions.

On the other hand, we conducted a separate set of experiments in well plates to elucidate how cerebral organoids alone respond to the administration of propofol and midazolam without the presence of BBB and mast cells. We measured *TNF-α* and glutamate levels in culture supernatants, analyzed organoid viability with WST-1 assay and the changes in specific gene-protein expressions with qRT-PCR and whole confocal imaging after vDISCO clearing (Supplementary Fig. 6, Supplementary Data 1p-t). Although the neuroinflammatory response defined by increased *TNF-α* levels after propofol administration and elevated glutamate levels with decreased organoid viability after midazolam administration were parallel to the platform results, this phenomenon was approximately twofold higher in our ICU patient-on-chip platform with the presence of endothelial cell function in the BBB barrier and the reactivation of mast cells in the neural tissue construct. Similarly, although there was no statistically significant differences (<2.5-fold) in the up-down regulation of most genes compared to the control group, we found that propofol led to significant increases only in *ITGAM* (5.8-fold) microglia and *NOS2* (2.8-fold) apoptotic gene expressions with significant decreases only in *IL10* (3.5-fold) and *MRC1* (5.75-fold) anti-inflammatory gene expressions, as expected. Moreover, we observed increases in *ITGAM* (8.3-fold) microglia and *ARG1* (2.6-fold) gene expressions with significant decreases only in *IL1B* (2.6-fold) gene expression in the midazolam administered group. Confocal microscopy images also support qRT-PCR results, as in addition to regional *GABA-A, vGLUT* and *MAP2* protein expression changes, only an increase in *CD11b+* microglia population was noticeable after sedative exposure. This result proved that the response to sedative exposure was different in the presence of mast cells and BBB endothelial cells. Thus, the ICU patient-on-a-chip platform, which we designed to recapitulate in vivo-like brain tissue with the BBB barrier, mast cells and cerebral organoids has provided a physiological integrity that can be used for translational studies.

Gene ontology enrichment analysis revealed the molecular pathways of sedative induced neuroinflammation processes

For further investigation of propofol and midazolam administrations on both cerebral organoids and mast cells, we conducted Gene Ontology (GO) and Kyoto Encyclopedia of Genes and Genomes (KEGG) Enrichment analyses to qRT-PCR genes. We examined the relationship between genes from qRT-PCR and all three GO terms cellular component (CC), molecular function (MF) and biological process (BP). About 42 GO terms were detected for the propofol administered organoids and 47 GO terms for the midazolam counterparts (Supplementary Data 2a,b).

When we examined the top enrichment GO terms of propofol group and related genes, "type 2 immune response", "immune systems process", and "nervous system development" GO terms showed *IL10, CD40, MRC1, ITGAM, IFNG, IFNB1, ARG1, GFAP, GABRA1, S100B, IL6* and *TNF* genes related neuroinflammation (Fig. 6a, b). In the midazolam group, the GO terms as "transmembrane signaling receptor activity", "signaling receptor activity" and "organic substance transport", also the genes as *ITGAM, MRC1, CD40, SLC17A7, GRIN1, CD40/80, ARG1, GFAP, GABRA1, IL6* and *IFNG* stood out (Fig. 6c, d). However, there were no significant KEGG enriched pathways for organoids in the groups administered with both propofol and midazolam (Supplementary Data 2c,d). For the mast cell qPCR results, we found 32 GO terms for propofol administered mast cells and 44 GO terms for midazolam counterparts (Supplementary Data 2e,f). When we examined the top enrichment GO terms of propofol administered mast cells and related genes, positive regulation of both "B cell mediated immunity" and "immunoglobuliıtgamn mediated immune response" were elicited, whereas negative regulation of "inflammatory response" GO terms showed propofol driven neuroinflammation effect and *CD40/80, GRIN1, IL12B, IFNG, IFNB1, TNF, STAT6, ARG1, IL1B, IL10,* and *IL13* genes were related to these GO terms (Fig. 7a, b). With respect to midazolam administered mast cells, the GO terms showed negative regulation of both "defense response", and "apoptotic signaling pathway", whereas positive

regulation of both "NF-kappaB transcription factor activity" and "T-helper cell differentiation" and the genes *IL13, IL10, IL12B, ENPP3, TNF, IFNB1, IL1A, IFNG, BCL2,* and *CD40/80* belonging to these GO terms stood out (Fig. 7c, d). In addition to GO, we found 2 and 6 significant KEGG enriched pathways for propofol and midazolam administered mast cells, respectively (Supplementary Data 2g, h). Among them, "NF-kappaB signaling pathway" for propofol (Supplementary Fig. 7a), and "Necroptosis pathway" for midazolam administered mast cells (Supplementary Fig. 7b) were the most important pathways to associate their relationship with neuroinflammation process.

Discussion

Physiologically functional mast cells that are characterized mainly with *CD203c, CD117, CD34* and *FceR1* markers, play important roles in the regulation of almost every part of the neuroinflammatory process by transforming from protective immune cells to pro-inflammatory cells[56,57]. Mast cells can be differentiated from a variety of stem cells including iPSCs via mesodermal differentiation and be used as a peripheral brain parenchyma tissue-resident immune cell in in vitro models to evaluate neuroinflammation[58,59]. In our study, we successfully differentiated *CD34/c-KIT/FES* higher expressed *CD203c+* mature mast cells from hiPSC. We then incorporated those into our easy to set, multi-layered and biomimetic ICU patient-on-a-chip platform that involves cerebral organoids derived from same origin iPSCs and hCMEC/D3 representing BBB and left the platform overnight to reach hemostasis. While sedatives are administered at various concentrations and durations, real-time analysis of the infusion of anesthesia in intensive care patients is not possible. This is important to determine the optimal sedative dose and maintain the continuity of anesthesia. To overcome this challenge, studies have examined the sedative concentrations of blood plasma from human blood. In one of these studies, the concentration of midazolam in blood plasma of a patient was reported to decrease to 0.2 μg/ml at the end of 1 hour, to whom intravenous midazolam was administered at a bolus dose of 0.2 mg/kg for induction of general anesthesia[60]. Another study focused on the concentrations of propofol in blood plasma and brain tissue. The initial plasma concentration of propofol was approximately 2.5 μg/ml and 3.5 μg/g in the brain. The plasma and brain concentrations decreased gradually with time, but the brain concentration was always higher than the plasma concentration[61]. Likewise, focusing on propofol concentrations in human plasma and brain tissue, concentrations in brain tissue were reported to be higher than plasma concentrations[62]. In our study, we administered sedatives at concentrations of 200 μM and 25 μM for propofol and midazolam, respectively, elicited as safety doses for endothelial cells. We repeated this administration on day 2 to evaluate the effects of prolonged sedative administration and harvested on day 4.

The immune cell-mediated potential neuroinflammatory and neurotoxic effect of sedative administration were evaluated by analyzing 4 different samples harvested from our on-chip platforms: (i) Permeability, TEER values and IF analysis of BBB construct, (ii) IF and qRT-PCR analysis of mast cells in the neural tissue construct, (iii) *TNF-α* and glutamate level analyses in culture supernatants, and finally, (iv) WST-1 tissue viability, qRT-PCR, whole confocal imaging after vDISCO clearing and TUNEL analyses of organoids in the neural tissue construct. The studies have shown the reactivation of mast cells in case of neuroinflammation were the earliest activators of BBB damage and precede both macroglial and microglial cell reactivation[63–65]. Therefore, we investigated the changes in the BBB integrity in terms of cell adhesion, junctions, permeability, TEER values and proinflammatory state, as well as the reactivation status of mast cells. The impaired barrier integrity with higher FITC permeability and lower TEER values due to decreases in *CD31* and *ZO-1* junctional complexes in endothelial cells and increase in the *TNF-α* expression levels after mainly midazolam administration, reveals the interactive nature between mast cells and BBB construct during mast cell mediated neuroinflammation. On the other hand, propofol exposure has not revealed such a significant alteration on BBB integrity and irregular mast cell reactivation, which is in agreement
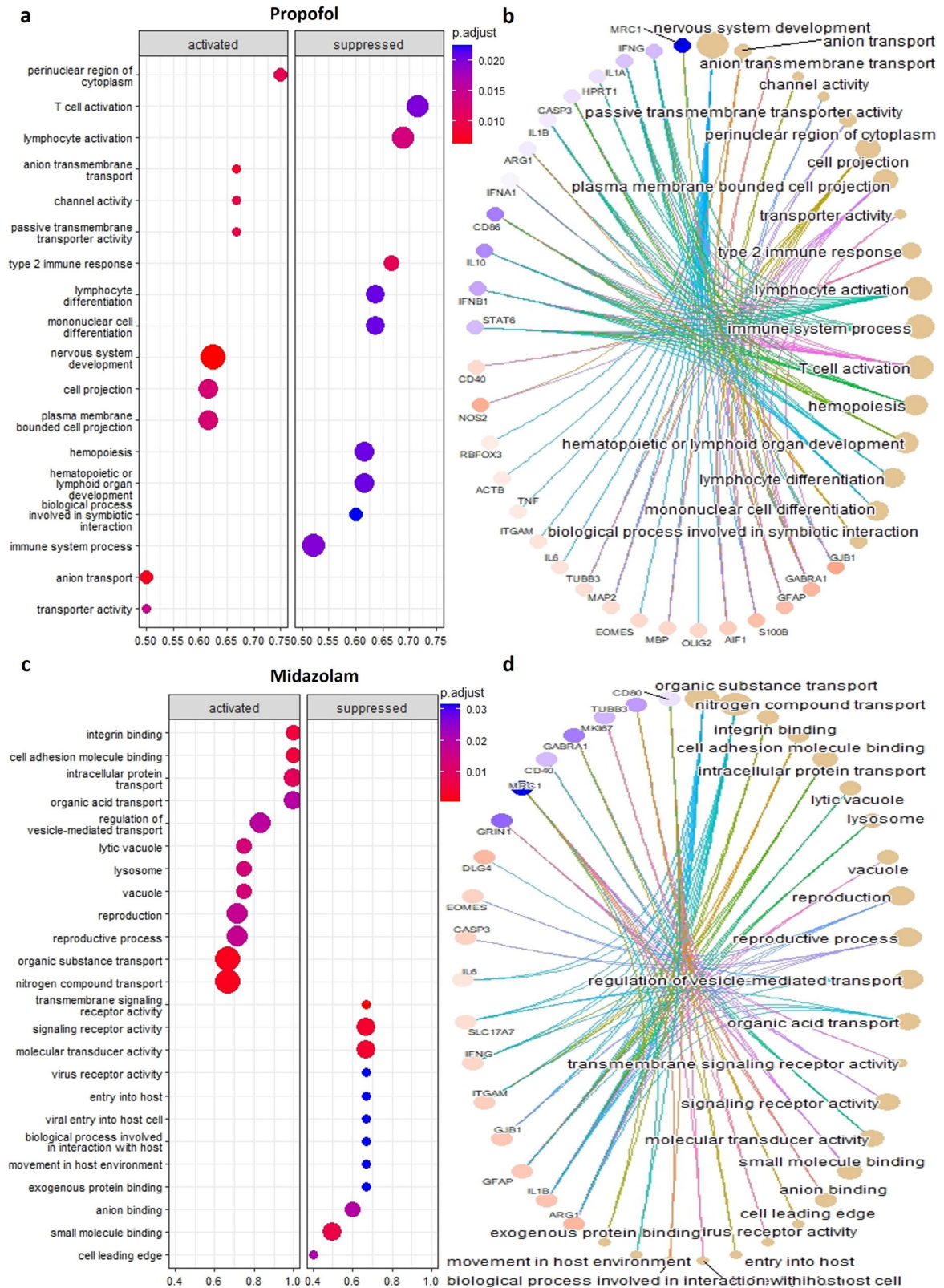
Fig. 6 | GO analysis of the target genes from qRT-PCR analyses of organoids. **a** Enriched all GO terms for upregulated (activated) and downregulated (suppressed) genes associated with propofol-administered organoids. **b** Genes related to enriched GO terms for propofol administered organoids **c** Enriched all GO terms for upregulated (activated) and downregulated (suppressed) genes associated with midazolam administered organoids **d** Genes related to enriched GO terms for midazolam administered organoids. (Red nodes indicate upregulated, blue nodes indicate downregulated genes in (**b**) and (**d**)).
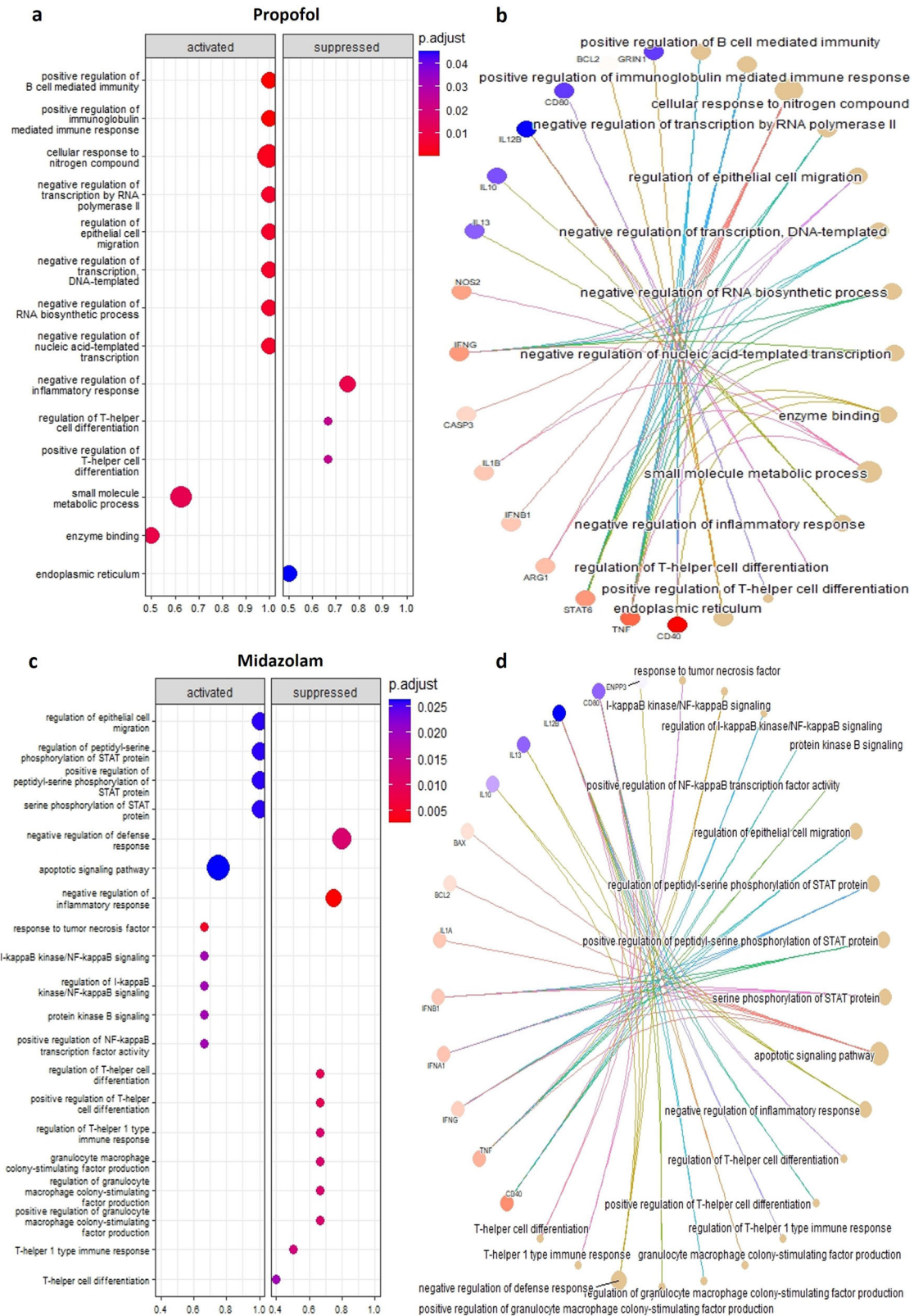
Fig. 7 | GO analysis of target genes from qRT-PCR analyses of mast cells.
a Enriched all GO terms for upregulated (activated) and downregulated (suppressed) genes associated with propofol-administered mast cells. **b** Genes related to enriched GO terms for propofol-administered mast cells. **c** Enriched all GO terms for upregulated (activated) and downregulated (suppressed) genes associated with midazolam-administered mast cells. **d** Genes related to enriched GO terms for midazolam-administered mast cells (Red nodes indicate upregulated, blue nodes indicate down-regulated genes in (**b**) and (**d**)).

with studies[36,66] noting that the effect of propofol on the BBB is not due to endothelial cell loss and adhesion.

Mast cells, as major resident immune cells in the brain, communicate with other CNS cells and mediate their reactivation as a pillar of the neuroinflammatory response. Reactivation of mast cells causes degranulation and release of inflammatory cytokines such as *TNF-α, IL-1β, IL-10* and *IL-33* stored in their granules[67]. The release and detection of *TNF-α* from mast cells, as an important indicator of active neuroinflammation related to proinflammatory response, precedes other resident cells in the CNS, including microglia and endothelial cells[68]. An earlier in vitro study showed that the inhibition of mouse bone marrow stem cell derived mast cell proliferation and *TNF-α* release, depend on administration time and dose of midazolam[69]. In our study, 25 μM of midazolam specifically increased *CD203c*+ activated mast cell proliferation. Furthermore, the higher expression level of *TNF-α* in both culture supernatants and mast cells after sedative administration, supported activated mast cell-related neuroinflammatory response, along with increased expression levels of proinflammatory genes; *CD40, TNF* and *NOS2*, and also decreased levels of anti-inflammatory genes; *IL12B, IL13,* and *IL10*. Recent studies have focused on investigating the long-term permanent damage caused by sedative exposure to the developing brain. Mimicking repetitive long-term administration, Xu et al. reported that midazolam administration to primary neuron culture for 72 h caused neuronal damage by inhibiting synaptogenesis in vitro[55], as consistent with reduced *vGLUT1* and *MAP2* levels observed in our on-chip organoids. Another study showed that 25 μM midazolam administration negatively affected oligodendrocyte lineage cells, myelin development, and action potentials by inhibiting the proliferation and migration of oligodendrocyte progenitor cells in the zebrafish dorsal spinal cord[70]. Notably, several studies mentioned that the activated brain mast cells aggravated neuroinflammation and neurotoxicity by reactivating both microglia and macroglia, and this abnormal event might directly induce neuronal cell apoptosis[71] due to secretion of high levels of neurotoxic molecules such as glutamate[2,72]. The destructive effects of sedatives, mostly midazolam, were evident via abnormal mast cell associated "Necroptosis pathway" in GO terms, and also glial cell reactivation in neural tissue construct in our on-chip platform. Importantly, we found 4-fold higher glutamate level in culture supernatants of midazolam administered group that suppressed organoid viability, decreased neuronal *MAP2/RBFOX3/TUBB3* gene expressions (2.8, 2.2 and 21.6-fold, respectively) and regionally reduced *MAP2*+ mature neuronal cell activity in organoids. In addition, *Ki-67-/TUNEL*+ and *CASP3* higher expressed tissue apoptosis was observed in organoids, presumably via destructive neurotoxic effect of reactivation of both proinflammatory mast cells, *CD11b*+ microglia and *GFAP* higher expressed macroglia. interestingly, midazolam administration increased organoid related genes such as forebrain specific *FOXG1*, postsynaptic specific *DLG4*, and *PAX6/EOMES higher expressed* progenitor cell proliferation genes, whereas propofol administration increased progenitor/mature neural/glial cell specific gene expression in cerebral organoids. Although this phenomenon appears to indicate a somehow protective effect of sedatives on the brain[73], the ever-increasing, excess number of both progenitor/mature neural/glial cells might also lead to a prolonged neuroinflammatory phenotype, which is a common feature in many neurodevelopmental disorders, but for different reasons.

Both microglial and macroglial cell reactivation and anti-homeostasis-mediated neuroinflammation are characterized by various approaches such as morphological analysis, cytokine release and changes in specific protein/gene expressions[2,74,75]. While the major increases in *IBA1* and *CD11b* expression levels indicate microglial reactivation, *GFAP* overexpression level contributes to macroglial cell fate, chiefly astrocyte reactivation[2,76] which is observed subsequent to sedative administration in our study. As the acute phase progresses to the subacute phase, neuroprotective microglia starts the healing phase of neuroinflammatory process, which induces *ARG1* expression with both *IL-10, IL-4* and *IL-13* cytokine-mediated anti-inflammatory responses that support injured tissue regeneration and CNS

repair[74,77]. Although we observed a notable increase in *ARG1* gene expression level (13.4-fold) in midazolam-administered organoids, generally high levels of pro-inflammatory and low levels of anti-inflammatory markers suggest that *CD11b*+ reactive microglia in the organoids could not acquire beneficial character and transitioned to the sub-acute phase for tissue repair. On the other hand, we found that the gene expression level of the *PSD95* postsynaptic marker, *DLG4*, significantly increased (12.4-fold) following midazolam administration. In this context, it is worth noting that *PSD95*is not only a glutamatergic neuronal postsynapse marker. A recent study showed the association of *PSD95*+ microglia in neuroinflammation-related brain damage in premature babies and argued that the role of *PSD95* protein in microglia might be related to a balance in Glutamatergic and GABAergic signaling or intercellular communication[78]. The group of *GABA* agonist sedatives, such as propofol and midazolam, positively modulate *GABA-A* receptor and may cause neurodegeneration in the early stages of development through impaired Ca2+ homeostasis[36–38]. On the other hand, previous studies indicate that sedative administration might activate *GABA-A* receptors, inhibit *NMDAR* receptors, modulate Ca2+ influx through slow calcium-ion channels, inhibit glutamate receptors and reduce extracellular glutamate levels, depending on dose and duration of administration[46,79,80]. Specifically in our ICU patient-on-a-chip platform, increased gene expression levels of *GABRA1* (both with *GABA-A* protein level), *GRIN1* (both with *NMDAR1* protein level) and *GJB1* with decreased protein levels of *vGLUT1* were identified in propofol administered organoids, that were associated to "type 2 immune response", "immune systems process", and "nervous system development" GO terms. However, decreased gene expression levels of *GRIN1* (both with *NMDAR1* protein level), *GABRA1* (both with *GABA-A* protein level), *SLC17A7* (both with *vGLUT1* protein level) and *GLS* with increased levels of only *GJB1* gene were noted in midazolam administered organoids, that were associated to the GO terms; "transmembrane signaling receptor activity", "signaling receptor activity" and "organic substance transport". The previous studies suggest that the dysregulated expression level of *GABA-A* receptors caused by sedatives contributes to post-operative cognitive dysfunction (POCD) characterized by memory and concentration problems, while anti-*GABA-A* receptors reduce POCD symptoms[81,82]. On the other hand, inflammatory cytokines secreted by reactivation of cerebral mast cells after anesthesia may cause POCD by causing BBB dysfunction[83] or reactivation of microglia[71]. Therefore, these results indicate different CNS immune cell reactivity in distinct neuroinflammation-based neuroimmune response pathways as a result of different mechanisms of action. Immuno-inflammatory conditions are homeostatically maintained biological processes to protect neural tissue in the CNS[2]. Therefore, understanding of the neuroinflammation process in which cells and cytokines have main roles, is important in neurodegenerative disorders and external influence-derived neurological pathologies. A recent study revealed that long-term sevoflurane exposure upregulated the levels of pro-inflammatory markers *TNF-α, IL-1β, IL-6,* and *iNOS* in the hippocampus, whereas downregulated the anti-inflammatory markers *IL-10, CD206,* and *ARG1*[84]. An important study conducted with ICU patients investigated the early immune response markers in the blood plasma after 48 h infusion of both propofol and midazolam. The results showed that while midazolam suppressed, propofol stimulated the expression of pro-inflammatory cytokines such as *IL-1β, IL-6* and *TNF-α*. Additionally, these two sedatives caused suppression of *IL-8* expression, while propofol inhibited *IL-2* and stimulated *IFN-γ* expression, whereas midazolam failed to do so, during 48 h of continuous infusion[85]. In our study, partly contrary, the proinflammation related genes; *NOS2, CD80, CD40, CD68, IL6* and *TNF* were increased with propofol, whereas *IL1B, IFNG, IFNA1* and *IL6* were increased with midazolam administration in cerebral organoids, along with a decreasing trend in anti-inflammatory related genes; *IL10, MRC1* and *STAT6,* (except *ARG1* in midazolam group), in both sedative administered tissue constructs. The reason for this difference might be related to the analyses of blood plasma of ICU patients, rather than the neural tissue directly as a readout, which highlights the importance of human complex tissue culture models for specific context of use.

The *CD40* receptor is a transmembrane protein that is critical to the initiation and sustainment of the inflammatory response, but the effects of its role in neurodegenerative diseases is still unclear. For this reason, *CD40* receptor has been studied in many neurodegenerative diseases such as multiple sclerosis (MS), Alzheimer's Disease (AD) and Parkinson's Disease (PD). *CD40* was reported to be associated with AD due to the damage to the surrounding neuronal tissue by the complex neurofibril structure (neurofibrillary tangles) formed as a result of *CD40* activation, and with PD due to dopaminergic neuron loss as a result of *CD40* dysregulation. The irregularly produced T and B cells due to disruptions in *CD40* and *CD40*-ligand interaction have been postulated to support MS pathology[86]. In addition, mast cells cultured with astrocytes can be stimulated to release other cytokines through *CD40* ligand interaction with *CD40* gene, supported by glial reactivation[87,88]. Thus, *CD40* gene expression levels of reactivated mast cells, which were increased with both sedative administrations in our ICU patient-on-a-chip platform, mostly in propofol (101.4-fold), are important in this context. Contrary to our expectations, *CD40* mRNA expression was downregulated in midazolam administered organoids (7.6-fold), possibly as a result of cell death. Conversely (and in line with our expectations), *CD40* mRNA levels showed an upregulation trend for propofol-administered organoids. *IFN-γ* has immunoregulatory effects and is important to generate an effective immune response. The ability of *IFN-γ* expression to induce *CD40* expression in human mast cells[89] is associated with different levels of increases in *CD40* gene. In ICU patients, *IFN-γ* was increased with propofol but not with midazolam administration[85]. In an in vitro study, the cell responses to *IFN-γ* injection were examined in the context of experimental autoimmune encephalomyelitis used to investigate MS mechanism. Low doses of *IFN-γ* protected microglia and oligodendrocytes against the disease, while high doses of *IFN-γ* further strengthened the disease effects in these cells[90]. In our ICU patient-on-a-chip platform, we found elevated *IFNG* gene expression in both propofol and midazolam-administered mast cells, like *CD40*. However, in organoids, we observed *IFNG* downregulation following propofol administration, compared to an upregulation following midazolam administration. In line with those observations, we found that propofol-administered organoids were more viable and *GFAP/S100B/OLIG2/MBP* higher expressed macroglial cell enriched, while midazolam-administered organoids were less viable, with *CD11b+* microglia enriched macroglia and secreted high levels of neurotoxic glutamate. Following that, we evaluated *CD80*, which is a cell membrane pro-inflammatory gene like *CD40*, responding to inflammatory stimuli. In a study examining the cortex, hippocampus, midbrain and striatum of mice treated with lipopolysaccharide, *CD80* expression was reported to increase in all four regions. Changes in *CD80* expression can activate and inhibit T cells. While T cells are activated by *CD80-CD28* interaction, *CD80* may cause an inhibitory effect on T cells by triggering *CTLA-4* and *PD-L1*[91]. Various studies have shown that the expression levels of *CD80* in human mast cells decrease due to inflammation, while the expression levels of *CD86* does not undergo a significant change[92,93]. Similarly, our results revealed no changes in *CD86* gene expression of mast cells, whereas *CD80* was downregulated in midazolam-administered organoids and both sedative-administered mast cells, unlike propofol-administered organoids.

Conclusion

The evaluation of long-term sedative administration to patients in ICUs is a complex and multifaceted challenge. For understanding the potential effects, risks, and benefits of sedative drugs in such scenarios, humanized microphysiological platforms can provide invaluable insights. In this study, we co-cultured the same genetic background hiPSCs differentiated mast cells and matured cerebral organoids in 3D matrix and supported with a membrane populated with hCMEC/D3 cells representing the BBB to form a humanized platform to study the effects of long-term sedative administration. We infused propofol and midazolam to ICU patient-on-a-chip and evaluated neural tissue and BBB layer constructs at the end of 4 days. Propofol administration activated *CD40* gene and *TNF-α* expression in mast cells, *AIF1* higher expressed microglia and *GFAP/S100B/OLIG2/MBP*

higher expressed macroglia, as well as caused *NOS2, CD80, CD40, CD68, IL6* and *TNF* genes mediated neuroinflammation in *GJB1* higher expressed *GABA-A+* and *NMDAR1+* cerebral organoids in the platform. On the other hand, midazolam administration activated mainly *CD40* higher expressed *CD203c+* proliferative mast cells, *CD11b+* microglia and *GFAP* higher expressed macroglia, as well as increased glutamate-related neurotoxicity, *IL1B, IFNG, IFNA1* and *IL6* genes mediated neuroinflammation in *DLG4GJB1* higher expressed and *GABA-A-/NMDAR1-* organoids and resulted in compromised BBB permeability and decreased TEER values with higher barrier disruption. All our results suggest that different sedative exposures cause variations in cell type activation that modulate different pathways related to neuroinflammation and neurotoxicity in our ICU patient-on-chip platform. While we have shown a connection between neurotoxicity and the administration of certain sedatives, quantification of glutamate levels in the culture supernatant using an off-chip kit was one of the approaches. However, embedding a sensor directly to the ICU patient-on-chip platform for in situ quantification of glutamate would be invaluable for acquiring real-time data. Non-enzymatic electrochemical sensors have been proposed for detecting glutamate[94,95]. On the other hand, typically, glutamate sensing is achieved through catalyzing the conversion of glutamate to produce hydrogen peroxide by glutamate oxidase[96]. The electrochemical activity of hydrogen peroxide on the working electrode can be employed to relate glutamate concentration to the current generated via amperometric measurement. Implementation of electrochemical glutamate sensors has been shown in vivo applications[97,98], with reduced sensitivity in prolonged operation[85]. The drift in detecting neurotransmitters as glutamate impedes the integration of these sensors to organ-on-a-chip platforms[99]. Our current focus involves the development of glutamate sensors to overcome these challenges and integrate them into organ-on-a-chip platforms. This approach significantly reduces the likelihood of false measurements, allowing for a more precise model. Additionally, the administration of stimulants and sedatives could be optimized using an on-chip drug delivery system. The system can be coupled with a secondary sensor to measure on-chip drug concentrations. Through a feedback loop, sedatives could be administered to achieve a time-dependent concentration profile, enhancing the accuracy of human mimicry. Consequently, a fully self-contained closed-loop digitized platform could be realized, facilitating a more precise modeling of neuroinflammation.

Materials and methods
Fabrication of ICU patient-on-a-chip platform
The ICU patient-on-a-chip platform was designed with the COMSOL multiphysics program as a multi-layered system that mimics the BBB supported neural tissue containing cerebral organoids and mast cells, which are resident immune cells of the CNS. The upper layer of the platform consists of the vascularization layer, which contains the fluid flow with co-culture media (1:1:1 ratio of endothelial cell, mast cell and cerebral organoid growth media). An interlayer was placed on top of the cerebral organoid chamber in which μ-platform matured 5 cerebral organoids were positioned on the micro concave structures of the platform and embedded into the matrigel containing mast cells. The collagen type I coated PET membrane seeded with hCMEC/D3 cells at a concentration of 1×10^5 cells/mL and incubated for 10 days to reach confluency, was sandwiched between the vascularization layer and the interlayer to mimic the BBB. Thus, while the BBB could be mimicked with fluid flow, a complete physiological microenvironment of neural tissue could be created with mast cells, cerebral organoids and hydrogel matrix (Fig. 1a). PDMS (SYLGARD 184), a biocompatible polymer, was used to create the main layers of ICU patient-on-a-chip platform. In this context, the PDMS-based elastomer was mixed with the curing in a ratio of 10:1 and the PDMS solution was obtained after removing the air bubbles using a vacuum pump. PDMS solution was poured into the Polymethylmethacrylate (PMMA) molds of the vascularization and interlayers obtained by laser cutting. The mold representing the neural tissue layer was obtained by using a 3D stereolithography printer and cured at 60 °C for 3–4 h. All layers were positioned on top of each other and clamped

with PMMA sheets by bolts and screws for liquid sealing. After overnight hemostasis of the model, sedatives were administered to the co-culture media at concentrations of 200 μM and 25 μM for propofol and midazolam, respectively as elicited safety doses for endothelial cells. The administration was repeated on day 2 and the cell-mediated immune responses were analyzed at the end of day 4.

The response of only cerebral organoids to the sedative administration without BBB and mast cells

A separate experiment was set up based on how cerebral organoids themselves response to the sedative exposure to propofol and midazolam. Briefly, after the maturation stage, organoids were transferred to well plates and we administered the elicited safety doses of 200 μM propofol and 25 μM midazolam in the cerebral diff media to the organoids on days 1 and 2. Then, we harvested the culture supernatants and organoids on day 4 for characterization.

3D computational fluid dynamics (CFD) simulation

Optimized initial conditions were investigated using 3D CFD simulation by Comsol Multiphysics to mimic the BBB and provide ideal microenvironment conditions around cerebral organoids. While the Brinkman equation was solved for flow conditions in the 3D matrix, the Navier-Stokes equation was solved for laminar flow conditions and velocity and shear stress profiles were analyzed.

hCMEC/D3 cell culture

hCMEC/D3 that were used for BBB construction, were obtained from Hacettepe University, Faculty of Medicine, Department of Histology and Embryology, Ankara, Turkey. Cells were cultured specifically in EGM-2 MV Microvascular Endothelial Cell Growth Medium-2 BulletKit (Lonza, CC-3202) on 50 μg/mL Collagen type I (Sigma-Aldrich, C9791) coated filtered cap T-flask in a humidified incubator with a 5% CO_2 at 37 °C. Collagen powder was dissolved in 0.1 M acetic acid at a concentration of 1 mg/mL and stored at 4 °C. Then, working concentration was prepared in HBSS, (Sigma-Aldrich, H9269) with phenol red at a ratio of 1:20. Confluence cells were passaged in every week using 0.05% Trypsin-EDTA (Sigma-Aldrich, T4049) and cryo stocks were taken in 10% DMSO (Sigma-Aldrich, D2650, USA) in fetal bovine serum (FBS, Sigma-Aldrich, F2442, USA).

hiPSCs maintenance

hiPSC lines, which were previously reprogrammed from human dermal fibroblasts of healthy donors and characterized in terms of pluripotency markers and mycoplasma purity, were obtained from Izmir Biomedicine and Genome Center, Stem Cell and Organoid Technologies Laboratory[26,100] The well-shaped iPSC colonies were passaged with 1 mg/mL dispase solution (StemCell Technologies, 07923, Canada) and cultured on matrigel matrix (Corning, 354230, USA) coated dishes with mTeSR1 medium (StemCell Technologies, 85857, Canada).

Mast cells differentiation from iPSCs

For the first stage of mast cell differentiation, the hematopoietic mesodermal differentiation in serum-free medium (SFM), iPSCs were seeded at a density of 10 colonies/well of matrigel coated 6-well plate and incubated for 4 days in 80 ng/mL BMP4 (Peprotech, 120-05ET, USA) supplemented mTeSR1 medium. The cells were then cultured in MC StemPro-1 medium (StemPro-34 SFM (Gibco, 10639011, USA) containing 1% NEAA (Sigma-Aldrich, M7145, USA), 2 mM L-glutamine (Sigma-Aldrich, G7513, USA), 0.5% penicillin/streptomycin (10,000 U-10 mg/mL, Sigma-Aldrich, P4333, USA), 80 ng/mL VEGF 165 (Sigma-Aldrich, GF315, USA), 25 ng/mL bFGF (Peprotech, 100-18B, USA) and 100 ng/mL SCF (Peprotech, 300-07, USA)) for 2 days. In the second stage, hematopoietic progenitor cells were cultured in MC StemPro-2 medium (StemPro-34 SFM containing 100 ng/mL SCF, 10 ng/mL IL-3 (Peprotech, 200-03, USA), 10 ng/mL thrombopoietin (TPO, Peprotech, 300-18, USA), 100 ng/mL IL-6 (Peprotech, 200-06, USA), 10 ng/

mL Fms-like tyrosine kinase 3 (FLT3, Peprotech, 300-19, USA), 1% NEAA, 2 mM L-glutamine and 0.5% penicillin/streptomycin) for hematopoietic progenitor cell expansion and initial myeloid differentiation with medium changing every 3–4 days. By approximately day 27 of culture, the floating hematopoietic progenitor cells (non adherent cells) were collected for either cryo stocks, fed back into main culture with in MC StemPro-2 medium or culturing as monolayer culture in MC monolayer medium (StemPro-34 SFM containing 100 ng/mL SCF, 10 ng/mL TPO, 100 ng/mL IL-6, 10 ng/mL FLT3, 1% NEAA, 2 mM L-glutamine, and 0.5% penicillin/streptomycin, without IL-3). The medium was replaced every 3–4 days and this process was continued for ~50 days for myeloid differentiation of floating cells, and for ~5 passages and around additional 4 weeks for monolayer cells to generate proliferative mature mast cells[58].

Characterization of mast cells

qRT-PCR analysis. iPSCs differentiated mast cells on day 27 (floating myeloid stage), 45 and 60 (more mature stage) were evaluated based on stemness; *SOX2, POU5F1 (OCT4), KLF4, MYC (c-MYC)* and mast cell specific; *CD34, PTPRC (CD45), ITGAM (CD11b), c-KIT (CD117), GJB1 (Connexin32), GRM1 (mGluR-1), GABRA1 (GABA-A), MIR9-1 (miR-9-5p), SLC17A7 (vGLUT1), FES (FceR1), GRIN1 (NMDAR)* genes (Supp. Table 1), compared to iPSCs. For this, total RNA isolation was performed from differentiated cells by using RNeasy Plus Mini Kit (Qiagen, 13323, Germany) according to the manufacturer's protocol. The concentrations of RNA were determined using a NanoDrop 1000 (Thermo Scientific) at wavelengths of 260/280 nanometers. Then, cDNA was synthesized from total RNA's utilizing the RT^2 First Strand cDNA Synthesis Kit (Qiagen, 330401, Germany). Then, qRT-PCR was performed for target genes using RT^2 SYBR Green qPCR Master Mix (Qiagen, 330503, Germany) via LightCycler 480 Instrument II (Roche, Germany). The gene expression level of each gene was normalized using *HPRT1, GAPDH,* and *ACTB* housekeeping genes, and data were analyzed utilizing the $2^{-\Delta\Delta CT}$ method to calculate fold changes in target gene expression. The heatmap graphs were drawn based on Log2 transformation of fold regulation using GraphPad Prism 8.3.0.

WB analysis. For determination of matured *CD203c* positive mast cells in culture, WB analysis was performed for 60 days of mast cells. For this, cell lysates were isolated by using RIPA lysis buffer (Thermo Fisher, 89901, USA) with protease-phosphatase inhibitor cocktail (1:100). After the amount of total protein was determined by BCA assay, separation of mast cells derived proteins according to their molecular weights was done by 10% sodium dodecyl sulfate-polyacrylamide gel (SDS-PAGE) and then transferred to a polyvinylidene difluoride (PVDF, Thermo Fisher, 88518, USA) membrane overnight at 4°C. Blot was blocked with blocking buffer (5% (w/v) skim milk in PBS-T) for 1 hour and labeled with 1:1000 diluted anti-*CD203c* and anti-*β-actin* (Thermo Scientific, MA1140, USA) primary antibodies in solution (10% (v/v) blocking buffer, 0.1% (w/v) sodium azide (Sigma-Aldrich, S8032, USA) in PBS-T) overnight on rocker shaker at +4 °C. After that, blot was incubated with horseradish peroxidase (HRP)-conjugated secondary antibodies (ProteinTech, SA00001-1 and SA00001-2, USA) for 1 hour at RT. Finally, Clarity Western ECL substrates in kit (Bio-Rad, 1705060, USA) were mixed at a ratio of 1:1 and applied to the membrane. Chemical reaction via bands were measured with a chemiluminescence imaging system containing a CCD camera (Bio-Rad, ChemiDoc MP Imaging System) at a wavelength of 428 nm.

IF staining. IF staining was performed to evaluate *CD203c* positive mature mast cell population in the differentiation process. For this, mast cells on day 30, 45 and 60 of culture were fixed with 4% (w/v) paraformaldehyde (PFA) at 4 °C for 30 min and washed three times with PBS and kept in PBS at 4°C until the time of staining. The fixed samples were permeabilized with 0.1% (v/v) Triton X-100 (Sigma-Aldrich, T8787, USA) for 15 min at room temperature (RT), blocked with 1% (w/v)

bovine serum albumin (BSA) solution (in PBS, GoldBio, A-421-25, USA) for 1 hour at RT. After blocking, samples were labeled with anti-*CD203c* primary antibodies (diluted in 1:300, Affinity, DF8517, USA) in antibody solution (3% (w/v) BSA and 0.025% (v/v) Triton X-100 in PBS at 4 °C overnight on shaker. After washing steps three times in PBS, samples were labeled with Alexa fluor 488-conjugated secondary antibody (diluted in 1:1000, Abcam, ab150077) for 1 hour at RT on shaker. Thereafter, cells were washed in PBS and stained with 1.5 µg/mL DAPI (in PBS, Sigma-Aldrich, D9542, USA) for 10 min at RT. At the end, cells were washed in PBS again, and mounted with a mounting medium (Thermo Fisher, P36961, USA) and visualized under a fluorescent microscope (Zeiss Axio Vert.A1).

µ-platform derived cerebral organoid formation. Early-stage cerebral organoids were generated as described in Lancaster method[101] and matured in µ-platforms as described in our previous study[26]. Briefly, embryoid bodies (EBs) were generated in hESC media (DMEM/F12 medium (Gibco) supplemented with 20% KOSR (Gibco, 10828028, USA), 3% hESC-qualified FBS (Gibco), 1% Glutamax (Gibco, 35050061, USA), 1% NEAA, 1% Penicillin/Streptomycin, 0.007% b-mercaptoethanol (55 mM, Sigma-Aldrich, M6250, USA) with 4 µg/mL bFGF and 50 µM Y-27632 Rock-inhibitor (Tocris, 1254, UK) from iPCSs seeded in ultra low attachment 96-well U-bottom well plate (Corning, 7007, USA) at 9000 cells/150 µL/well. At the end of the 6th day, EBs were transferred to ultra low attachment 24-well plates and neural epithelial structures were formed in neural induction medium ((DMEM/F12 medium (Gibco, 31330038, USA) with 1% N2 supplement (Gibco), 1% Glutamax, 1% MEM-NEAA, 1% penicillin/streptomycin, and 1 µg/mL Heparin (Stem Cell Technologies) for additional 5 days. Then, EBs were embedded in the matrigel matrix at day 11 and cultured in the cerebral organoid differentiation medium (1:1 ratio of DMEM-F12 and neurobasal medium (Gibco, 21103049, USA) supplemented with 0.5% N2 supplement (Gibco, 17502048, USA), 0.025% Insulin (Sigma-Aldrich, I9278, USA), 1% Glutamax, 0.5% NEAA, 1% penicillin–streptomycin, 0.035% b-mercaptoethanol (1:100 in medium), and 1% B27 supplement without vitamin A (Gibco, 12587010, USA)) for additional 4 days until many neuroepithelial buds were formed. At the end of the 15th day, early-stage organoids were transferred to hemispherical wells of PDMS-based µ-platforms that connected in series. Hydraulic tightness was achieved by tightening the PMMA sheets positioned on both upper and bottom sides of the platform with screws and bolts. The cerebral organoid maturation medium supplemented with B27 vitamin A (Gibco, 17504044, USA) in the system reservoir, was circulated with a peristaltic pump (Longer pump, BT100-2J). The µ-platform based organoid maturation was maintained under dynamic conditions in incubators at 37 °C with 5% CO_2 for additional 60 days, for functional-molecular maturity with a non-variable manner.

Cellular, molecular and functional effects of sedatives on ICU patient-on-a-chip

Determination of safety doses of sedatives. To compare the concentrations of clinical, in vivo and in vitro sedative administration, the dose-dependent (400, 200, 100, 50, 25, 12.5, 6.25, 3.3 µM) propofol and midazolam administration were carried out to hCMEC/D3 cells in 2D in vitro culture in order to determine the safety-doses for ICU patient-on-a-chip platform. Within this scope, hCMEC/D3 cells were seeded at a density of 1×10^4 cells/100 µL/well into collagen type I coated 96-well TC plates. After 24 h incubation, various concentrations of both propofol and midazolam as test groups, culture medium as a positive control and DMSO as a negative control were added to each well and incubated for 4 days. Thereafter, the cell supernatants were removed, 100 µL of 10% MTT solution (in SFM from 5 mg/mL stock, Sigma-Aldrich, M5655, USA) was added to each well and incubated for 3 h at 37 °C in the dark. Then, MTT was removed and DMSO was added to the wells to solve formazan crystals. Optical density (OD) at 570 nm was measured using a microplate reader. Cytotoxicity that was quantified according to

percentage cell viability values were determined with GraphPad Prism 8.3.0 software.

Permeability assay. The effect of sedative treatment on BBB integrity mimicked by seeding hCMEC/D3 endothelial cells on PET membrane was evaluated with FITC permeability assay. In this context, endothelial cells were seeded at 1×10^5 cells/mL concentration in 250 µL on collagen type I coated 24-well PET membrane cell culture insert (Greiner bio-one, 662630, USA). After 10 days for barrier integrity, the sedative treatments were carried out under dynamic conditions for 4 days by applying repeated doses on day 2, in accordance with the safety-doses in the ICU patient-on-a-chip platform. After incubation, culture medium was removed and 100 µL of 10 mM FITC solution (F7250, Sigma-Aldrich, USA) diluted in HEPES solution (1 mM, diluted in PBS) added to the apical side (A) of the insert and, 600 µL of HEPES solution was added to the basolateral side (B). After 60 min of FITC solution passed through the models, 100 µL of samples were taken from the basolateral side and measured at 428–530 nm on a fluorospectrometer (Varioskan Lux, Thermo Fisher USA). FITC permeability (*P*) values (cm/s) from the barrier were obtained with the related Eq. (1) (where *V* is the volume of the media in the B side in cm³, *A* is the cross-sectional surface area of the insert membrane in cm², and *C* is the concentration of the A side in g/mL, delC is the concentration change over time of the B side in g/mL, del t is the passing time in second) by using the concentration values corresponding to the fluorescence values determined using the calibration plot of the FITC solution (Supplementary Fig. 4a, Supplementary Data 1c).

$$P\left(\frac{cm}{s}\right) = \frac{V(cm^3)}{A(cm^2)x[C]_A\left(\frac{g}{mL}\right)} x \frac{\Delta[C]_B\left(\frac{g}{mL}\right)}{\Delta t(s)} \qquad (1)$$

TEER measurement. The effect of sedative administration on BBB integrity was ascertained with TEER measurement as well. For this, hCMEC/D3 endothelial cells were seeded at a concentration of 1×10^5 cells/mL on the apical side of collagen type I coated six-well PET membrane cell culture insert (Greiner bio-one, 657630, USA). After 10 days for barrier integrity, the sedative treatments were carried out under dynamic conditions for 4 days by applying repeated doses on day 2, in accordance with the safety-doses in the ICU patient-on-a-chip platform. After incubation, the culture medium was refreshed. STX4 electrodes were cleaned by placing the tips of the probe in 70% ethanol and PBS, and then equilibrated for 15 min in endothelial cell culture medium at RT. The STX4 probe was then connected to an EVOM™ Manual (World Precision Instruments, EVM-MT-03-01, UK) and inserted into the transwell insert, stably. The longer part of the electrode was positioned to gently touch the bottom of the plate, whilst the shorter electrode rested slightly above the insert dish, not making contact with the hCMEC/D3 cell layer. Resistance values were reported as recorded values for each replicate minus the resistance of cell-free inserts (~55–70, variable according to different culture medium) measured alone. The values were then multiplied by 4.53 to address the cell culture insert area (cm²). Readings were repeated three times to ensure reproducibility.

IF staining. hCMEC/D3 cells were freshly fixed on chip membrane with PFA at 4 °C for 1 hour. And, mast cells embedded in a 3D matrix were firstly removed from matrigel with cold PBS washing and centrifugation. Then, isolated cells were monolayered on matrigel coated plates. After 3 days, mast cells were fixed for 30 min at 4 °C with 4% PFA. After fixation steps, IF staining of both mast cells and hCMEC/D3 cells was carried out as previously described based on anti-*CD203c* primary antibody (Affinity, DF8517, 1:300) for mast cells, and anti-*ZO1* (Abcam, ab96587, 1:300) and anti-*CD31* (SantaCruz, sc-376764, 1:200) primary antibodies for hCMEC/D3 cells overnight at 4 °C. Finally, the samples were washed three times with 1× PBS and labeled with secondary antibodies (Alexa fluor 488 and 594 conjugated and diluted in the blocking buffer at 1:1000) at RT for 1 hour. After the last washing step, the samples were covered

with DAPI containing mounting media, and imaged with confocal microscopy (Zeiss LSM 880).

WST-1 assay. Cell proliferation analyses of organoids in on-chip platforms were quantitatively performed with the WST-1 test based on formazan crystals released due to mitochondrial activity. Following the 1:10 rule found in the WST 1 analysis, 200 µL of nutrient medium/20 µL of reagent was added to each group. Then, the absorbance values of the organoids incubated at 37 °C for 2 h were obtained with a fluorescent microplate reader.

ELISA assay. The *TNF-α* mediated neurotoxic effect of sedatives in ICU patient-on-a-chip platforms was examined by determining the amount of *TNF-α* in the supernatant collected from the platform at the end of the 4th day, by following the standard protocols of the human *TNF-α* ELISA kit (EH0302, FineTest).

Glutamate assay. Releasing glutamate levels from ICU patient-on-a-chip platform after sedative administrations were evaluated for the immune cell-mediated neurotoxic effect of sedatives. In this context, after 4 days of treatment, the supernatants of the platforms were collected and analyzed with the colorimetric glutamate kit (MAK330-1K, Sigma-Aldrich) according to the manufacturer's instructions. Glutamate levels (mM) were quantitatively analyzed by GraphPad Prism 8.3.0 program via standard curve (Supplementary Fig. 4b, Supplementary Data 1i).

qRT-PCR analysis. Total RNAs were extracted from both mast cells and cerebral organoids from on-chip platforms. The qRT-PCR analysis was performed for target genes including proinflammatory; *TNF (TNF-α), IL6 (IL-6), NOS2 (Inos), CD40, CD68, CD80, CD86, IL1A (IL-1α), IL1B (IL-1β), IFNA1 (IFN-α), IFNB1 (IFN-β), IFNG (IFN-γ)*, anti-inflammatory; *IL5 (IL-5), IL10 (IL-10), IL12B (IL-12), IL13 (IL-13), MRC1 (CD206), STAT6, ARG1* and non-inflammatory related; *ENPP3 (CD203c), SLC17A7, FES, GRIN1, CASP3 (Caspas3), c-KIT, CD34, GLS (Glutaminase), BCL2 (BAX), GJB1, PTPRC, GRM1, GABRA1, MIR9-1, MKI67 (Ki67), CASP3* genes for mast cells, and also neural/glial cell type specific; *MAP2, RBFOX3 (NEUN), OLIG2, MBP, GFAP, S100B, ITGAM, AIF1 (IBA1)*, non-inflammatory releated; *TUBB3 (TUJ1), PAX6, EOMES (TBR2), FOXG1, DLG4 (PSD95), GRIN1, GLS, GJB1, SLC17A7, GABRA1*, proinflammatory; *TNF, IL6, NOS2, CD40, CD68, CD80, IL1A, IL1B, IFNA1, IFNB1, IFNG* and anti-inflammatory: *IL10, MRC1, STAT6, ARG1*, genes for organoids (Supplementary Table S1) as previously described.

Tissue clearing. The organoids in the ICU patient-on-a-chip platforms with and without sedative administered groups carried out under dynamic conditions were evaluated with the 3D vDISCO tissue clearing method to monitor changes in protein levels. For this, cerebral organoids embedded in a 3D matrix in the platform were fixed with 4% PFA for 2 h at 4 °C, after cold PBS washing for matrigel removal. Then, washed with PBT solution (0.1% (v/v) Tween-20 in PBS) 3 times for 30 min and incubated overnight at 4 °C. The next day, samples were blocked in iMarika solution (10% FBS, 2% BSA, 0.05% sodium azide (Sigma-Aldrich, 71290, USA), 0.5% Triton-X 100 and 5% DMSO in PBT) for 6 h at 4 °C. Then, anti-*FOXG1* (Abcam, ab18259, 1:500), anti-*SOX2* (Millipore, SC1002, 1:500), anti-*TUJ1* (Novus, NB100-161, 1:500), anti-*SATB2* (Abcam, ab51502, 1:500), anti-*CTIP2* (Abcam, ab18465, 1:500), anti-*PAX6* (Thermo, 426600, 1:500), anti-*CD11b* (Abcam, ab8878, 1:500), anti-*GFAP* (Affinity, DF6040, 1:200), anti-*OLIG2* (IBL, 18953, 1:500), anti-*MAP2* (Abcam, ab5392, 1:500), anti-*vGLUT1* (Thermo Scientific, 48-2400, 1:500), anti-*NMDAR1* (Affinity, AF6406, 1:200), anti-*GABA-A* (Affinity, Ab6207, 1:200) and anti-*Ki67* (SantaCruz, sc-23900, 1:500) primary antibodies were diluted in the iMarika solution and samples were incubated in it on a shaker at 4 °C for 3 days. After washing with iMarika

solution three times for an hour at +4 °C, the organoids were labeled with secondary antibodies (Alexa fluor 488, 594 and 647 conjugated) diluted in iMarika solution (1:1000) on a shaker at 4 °C for additional 3 days. Thereafter, the organoids were washed with iMarika solution three times for an hour at +4 °C and were stained with DAPI solution diluted 1:3000 in iMarika solution at RT for an hour. After the washing steps 2 times in iMarika solution and in PBS, samples were left in PBS until the dehydration and clearing steps. For the dehydration step, labeled organoids were first kept in 50% Tetrahydrofuran (THF, Sigma-Aldrich, 186562, USA) solution in water overnight, and they were passed through a series of 50%, 70%, 90% and 100% THF solution in water for an hour each. Then, they were kept in 100% THF again overnight. The next day, dehydrated organoids were incubated in a dichloromethane solution (Sigma-Aldrich, 270997, USA) in corrosion-resistant polypropylene tubes under a hood for ~15 min until collapse. Then, the samples were cleared repeatedly in ethyl cinnamate solution (Sigma-Aldrich, 66761, USA) for 3 h to transparency of the tissue. In the final stage, image analysis of whole organoids (without sectioning) in this solution was performed by confocal microscopy (Zeiss LSM880)[102–104].

TUNEL apoptosis test. To examine apoptotic regions in sedative-administered organoids in ICU patient-on-a-chip platform, DeadEnd™ Fluorometric TUNEL System (Promega, G3250) assay was carried out. For this, the paraffin-embedded sections of organoids were washed twice in xylene, 1× PBS, 100% ethanol, ethanol dilutions down to 50%, and 0.85% NaCl for 5 min. After rewashing in PBS, sections were incubated in 4% formaldehyde for 15 min, washed in PBS again and 20 µg/mL Proteinase K was dropped on samples for 10 min. After the 4% formaldehyde step was repeated, the positive control group was treated with 1× DNAse solution. Then, sections were equilibrated with a 100 µL equilibration buffer for 10 min at RT, were labeled with 50 µL of TdT reaction mix, and incubated for 60 min at 37 °C in a humidified chamber in the dark. To stop the reaction, sections were washed in 2× SSC for 15 min and in PBS for 5 min. Finally, to visualize all nuclei in tissue, sections were stained with 1:1000 DAPI for 10 min, washed in PBS again, and mounted with mounting medium, and the localized green fluorescence of apoptotic cells in tissue was detected by fluorescence microscopy (Zeiss, Axio Vert.A1).

GO and KEGG enrichment analysis. Functions 'gseGO and 'gseKEGG in R package 'clusterprofiler v4.8.3' were used for GO and KEGG analysis of target genes of qRT-PCR[105]. All GO terms (CC, MF, and BP) were selected. The parameters minimum genesets size, maximum genesets size and *p* value were set 3, 800 and 0.05, respectively. To visualize GO and KEGG results, functions 'dotplot and 'cnetplot and R package pathview' were used.

Statistics and reproducibility. All data are representative of at least two different biological replicates and were statistically analyzed by one-way or two-ways ANOVA, Tukey's or Dunnett's multiple comparisons test with ±95% confidence interval and *p* values < 0.05 were considered statistically significant in GraphPad Prism 8.3.0 program. Data was presented as the mean ± standard deviation with individual data points. In order to indicate degree of significance, ns; *p* > 0.05, **p* < 0.05, ***p* < 0.01, ****p* < 0.001, *****p* < 0.0001 were used. The Student's *t* test was also used for qRTPCR analysis (independent replicates = 2 with RNA isolate pool containing at least two samples from the same batch).

Reporting summary
Further information on research design is available in the Nature Portfolio Reporting Summary linked to this article.

Data availability
The source data behind the graphs in the paper can be found in Supplementary Data 1.

Code availability

References
1. Diaz-Castro, B., Bernstein, A. M., Coppola, G., Sofroniew, M. V. & Khakh, B. S. Molecular and functional properties of cortical astrocytes during peripherally induced neuroinflammation. *Cell Rep.* **36**, 109508 (2021).
2. Saglam-Metiner, P., Duran, E., Sabour-Takanlou, L., Biray-Avci, C. & Yesil-Celiktas, O. Differentiation of neurons, astrocytes, oligodendrocytes and microglia from human induced pluripotent stem cells to form neural tissue-on-chip: a neuroinflammation model to evaluate the therapeutic potential of extracellular vesicles derived from mesenchymal stem cells. *Stem Cell Rev. Rep.* **20**, 413–436 (2024).
3. Hendriksen, E., van Bergeijk, D., Oosting, R. S. & Redegeld, F. A. Mast cells in neuroinflammation and brain disorders. *Neurosci. Biobehav. Rev.* **79**, 119–133 (2017).
4. Cecen, B. et al. Biosensor integrated brain-on-a-chip platforms: progress and prospects in clinical translation. *Biosens. Bioelectron.* **225**, 115100 (2023).
5. Kempuraj, D. et al. Brain and peripheral atypical inflammatory mediators potentiate neuroinflammation and neurodegeneration. *Front. Cell Neurosci.* **11**, 216 (2017).
6. Kempuraj, D. et al. Neuroinflammation induces neurodegeneration. *J. Neurol. Neurosurg. Spine* **1**, 1003 (2016).
7. Dong, H., Zhang, X. & Qian, Y. Mast cells and neuroinflammation. *Med. Sci. Monit. Basic Res.* **20**, 200–206 (2014).
8. Germundson, D. L. & Nagamoto-Combs, K. Potential role of intracranial mast cells in neuroinflammation and neuropathology associated with food allergy. *Cells* **11**, 738 (2022).
9. Mittal, A., Sagi, V., Gupta, M. & Gupta, K. Mast cell neural interactions in health and disease. *Front. Cell Neurosci.* **13**, 110 (2019).
10. Dong, H. et al. Suppression of brain mast cells degranulation inhibits microglial activation and central nervous system inflammation. *Mol. Neurobiol.* **54**, 997–1007 (2017).
11. Dong, H. et al. Stabilization of brain mast cells alleviates LPS-induced neuroinflammation by inhibiting microglia activation. *Front. Cell Neurosci.* **13**, 191 (2019).
12. Kwon, H. S. & Koh, S.-H. Neuroinflammation in neurodegenerative disorders: the roles of microglia and astrocytes. *Transl. Neurodegener.* **9**, 42 (2020).
13. Ormel, P. R. et al. Microglia innately develop within cerebral organoids. *Nat. Commun.* **9**, 4167 (2018).
14. Toma, K., Wang, T. & Hanashima, C. Encoding and decoding time in neural development. *Dev. Growth Differ.* **58**, 59–72 (2016).
15. Fair, S. R. et al. Electrophysiological maturation of cerebral organoids correlates with dynamic morphological and cellular development. *Stem Cell Rep.* **15**, 855–868 (2020).
16. Sun, N. et al. Applications of brain organoids in neurodevelopment and neurological diseases. *J. Biomed. Sci.* **28**, 30 (2021).
17. Mak, I. W., Evaniew, N. & Ghert, M. Lost in translation: animal models and clinical trials in cancer treatment. *Am. J. Transl. Res.* **6**, 114–118 (2014).
18. Cui, X., Hartanto, Y. & Zhang, H. Advances in multicellular spheroids formation. *J. R. Soc. Interface* **14**, 20160877 (2017).
19. Peng, H., Harvey, B. T., Richards, C. I. & Nixon, K. Neuron-derived extracellular vesicles modulate microglia activation and function. *Biology* **10**, 948 (2021).
20. Ao, Z. et al. Tubular human brain organoids to model microglia-mediated neuroinflammation. *Lab Chip* **21**, 2751–2762 (2021).
21. Bang, S., Lee, S., Choi, N. & Kim, H. N. Emerging brain-pathophysiology-mimetic platforms for studying neurodegenerative diseases: brain organoids and brains-on-a-chip. *Adv. Healthc. Mater.* **10**, e2002119 (2021).
22. Yaldiz, B., Saglam-Metiner, P., Cam, S. B., Korkusuz, P. & Yesil-Celiktas, O. Effect of sterilization methods on the mechanical stability and extracellular matrix constituents of decellularized brain tissues. *J. Supercrit. Fluids* **175**, 105299 (2021).
23. Ingber, D. E. Human organs-on-chips for disease modelling, drug development and personalized medicine. *Nat. Rev. Genet.* **23**, 467–491 (2022).
24. Lancaster, M. A. et al. Cerebral organoids model human brain development and microcephaly. *Nature* **501**, 373–379 (2013).
25. Pașca, S. P. et al. A nomenclature consensus for nervous system organoids and assembloids. *Nature* **609**, 907–910 (2022).
26. Saglam-Metiner, P. et al. Spatio-temporal dynamics enhance cellular diversity, neuronal function and further maturation of human cerebral organoids. *Commun. Biol.* **6**, 173 (2023).
27. Cho, A. N. et al. Microfluidic device with brain extracellular matrix promotes structural and functional maturation of human brain organoids. *Nat. Commun.* **12**, 4730 (2021).
28. Sabate-Soler, S. et al. Microglia integration into human midbrain organoids leads to increased neuronal maturation and functionality. *Glia* **70**, 1267–1288 (2022).
29. Muhlhofer, W. G. et al. Duration of therapeutic coma and outcome of refractory status epilepticus. *Epilepsia* **60**, 921–934 (2019).
30. Dolinay, T. et al. Ventilator weaning in prolonged mechanical ventilation—a narrative review. *J. Clin. Med.* **13**, 1909 (2024).
31. Griffin, C. E., Kaye, A. M., Bueno, F. R. & Kaye, A. D. Benzodiazepine pharmacology and central nervous system-mediated effects. *Ochsner J.* **13**, 214–223 (2013).
32. Sahinovic, M. M., Struys, M. M. R. F. & Absalom, A. R. Clinical pharmacokinetics and pharmacodynamics of propofol. *Clin. Pharmacokinet.* **57**, 1539–1558 (2018).
33. Slingerland-Boot, R., Kummerow, M., Arbous, S. M. & van Zanten, A. R. H. Association between first-week propofol administration and long-term outcomes of critically ill mechanically ventilated patients: a retrospective cohort study. *Clin. Nutr.* **43**, 42–51 (2024).
34. Singh, A. & Anjankar, A. P. Propofol-related infusion syndrome: a clinical review. *Cureus* **14**, e30383 (2022).
35. Jurd, R. et al. General anesthetic actions in vivo strongly attenuated by a point mutation in the GABA(A) receptor beta3 subunit. *FASEB J.* **17**, 250–252 (2003).
36. Hughes, J. M. et al. The effects of propofol on a human in vitro blood-brain barrier model. *Front. Cell Neurosci.* **16**, 835649 (2022).
37. Twaroski, D. M., Yan, Y., Olson, J. M., Bosnjak, Z. J. & Bai, X. Down-regulation of MicroRNA-21 Is involved in the propofol-induced neurotoxicity observed in human stem cell-derived neurons. *Anesthesiology* **121**, 786–800 (2014).
38. Bosnjak, Z. J., Logan, S., Liu, Y. & Bai, X. Recent insights into molecular mechanisms of propofol-induced developmental neurotoxicity: implications for the protective strategies. *Anesth. Analg.* **123**, 1286–1296 (2016).
39. Zheng, J. et al. Midazolam ameliorates impairment of the blood–brain barrier (BBB) against LPS. *Neurotox. Res.* **40**, 751–762 (2022).
40. Han, X. et al. The protective effect of propofol on ionizing radiation-induced hematopoietic system damage in mice. *RSC Adv.* **9**, 36366–36373 (2019).
41. Li, X., Yao, L., Liang, Q., Qu, H. & Cai, H. Propofol protects hippocampal neurons from hypoxia-reoxygenation injury by decreasing calcineurin-induced calcium overload and activating YAP signaling. *Oxid. Med. Cell Longev.* **2018**, 1–12 (2018).
42. Dominguini, D. et al. The effects of anaesthetics and sedatives on brain inflammation. *Neurosci. Biobehav. Rev.* **127**, 504–513 (2021).

43. Lim, W. F., Inoue-Yokoo, T., Tan, K. S., Lai, M. I. & Sugiyama, D. Hematopoietic cell differentiation from embryonic and induced pluripotent stem cells. *Stem Cell Res. Ther.* **4**, 71 (2013).

44. Crupi, R., Impellizzeri, D. & Cuzzocrea, S. Role of metabotropic glutamate receptors in neurological disorders. *Front. Mol. Neurosci.* **12**, 20 (2019).

45. Harcha, P. A. et al. Mast cell and astrocyte hemichannels and their role in Alzheimer's disease, ALS, and harmful stress conditions. *Int J. Mol. Sci.* **22**, 1924 (2021).

46. Wen, Y. et al. Glutamate and GABAA receptor crosstalk mediates homeostatic regulation of neuronal excitation in the mammalian brain. *Signal. Transduct. Target. Ther.* **7**, 340 (2022).

47. Mayoral, R. J. et al. MicroRNA-221–222 regulate the cell cycle in mast cells. *J. Immunol.* **182**, 433–445 (2009).

48. Fenger, J. M. et al. Overexpression of miR-9 in mast cells is associated with invasive behavior and spontaneous metastasis. *BMC Cancer* **14**, 84 (2014).

49. Alim, M. A. et al. Increased mast cell degranulation and co-localization of mast cells with the NMDA receptor-1 during healing after Achilles tendon rupture. *Cell Tissue Res* **370**, 451–460 (2017).

50. Fodale, V. & La Monaca, E. Propofol infusion syndrome. *Drug Saf.* **31**, 293–303 (2008).

51. Goksel, O. et al. Comprehensive analysis of resilience of human airway epithelial barrier against short-term PM2.5 inorganic dust exposure using in vitro microfluidic chip and ex vivo human airway models. *Allergy* https://doi.org/10.1111/all.16179 (2024).

52. Sandhu, J. K. & Kulka, M. Decoding mast cell-microglia communication in neurodegenerative diseases. *Int. J. Mol. Sci.* **22**, 1093 (2021).

53. Ormel, L., Stensrud, M. J., Bergersen, L. H. & Gundersen, V. VGLUT1 is localized in astrocytic processes in several brain regions. *Glia* **60**, 229–238 (2012).

54. Rodriguez-Perdigon, M. et al. Down-regulation of glutamatergic terminals (VGLUT1) driven by Aβ in Alzheimer's disease. *Hippocampus* **26**, 1303–1312 (2016).

55. Xu, J. et al. Early developmental exposure to repetitive long duration of midazolam sedation causes behavioral and synaptic alterations in a rodent model of neurodevelopment. *J. Neurosurg. Anesthesiol.* **31**, 151–162 (2019).

56. Grootens, J., Ungerstedt, J. S., Nilsson, G. & Dahlin, J. S. Deciphering the differentiation trajectory from hematopoietic stem cells to mast cells. *Blood Adv.* **2**, 2273–2281 (2018).

57. Ribatti, D. & d'Amati, A. Hematopoiesis and mast cell development. *Int J. Mol. Sci.* **24**, 10679 (2023).

58. Igarashi, A. et al. Mast cells derived from human induced pluripotent stem cells are useful for allergen tests. *Allergol. Int.* **67**, 234–242 (2018).

59. Luo, Y. et al. A novel approach for studying mast cell–driven disorders: mast cells derived from induced pluripotent stem cells. *J. Allergy Clin. Immunol.* **149**, 1060–1068.e4 (2022).

60. Miyake, W. et al. Electroencephalographic response following midazolam-induced general anesthesia: relationship to plasma and effect-site midazolam concentrations. *J. Anesth.* **24**, 386–393 (2010).

61. Kawata, M. et al. Development of extended pharmacokinetic models for propofol based on measured blood and brain concentrations. *Sci. Rep.* **14**, 6326 (2024).

62. Van Hese, L., Theys, T., Absalom, A. R., Rex, S. & Cuypers, E. Comparison of predicted and real propofol and remifentanil concentrations in plasma and brain tissue during target-controlled infusion: a prospective observational study. *Anaesthesia* **75**, 1626–1634 (2020).

63. Wang, Y. et al. The mast cell is an early activator of lipopolysaccharide-induced neuroinflammation and blood-brain barrier dysfunction in the hippocampus. *Mediators Inflamm.* **2020**, 8098439 (2020).

64. Versele, R., Sevin, E., Gosselet, F., Fenart, L. & Candela, P. TNF-α and IL-1β modulate blood-brain barrier permeability and decrease amyloid-β peptide efflux in a human blood-brain barrier model. *Int. J. Mol. Sci.* **23**, 10235 (2022).

65. Takata, F., Nakagawa, S., Matsumoto, J. & Dohgu, S. Blood-brain barrier dysfunction amplifies the development of neuroinflammation: understanding of cellular events in brain microvascular endothelial cells for prevention and treatment of BBB dysfunction. *Front. Cell Neurosci.* **15**, 661838 (2021).

66. Längrich, T. et al. Disturbance of key cellular subproteomes upon propofol treatment is associated with increased permeability of the blood-brain barrier. *Proteomes* **10**, 28 (2022).

67. Iskarpatyoti, J. A. et al. Mast cell regranulation requires a metabolic switch involving mTORC1 and a glucose-6-phosphate transporter. *Cell Rep.* **40**, 111346 (2022).

68. Jin, Y., Silverman, A. J. & Vannucci, S. J. Mast cells are early responders after hypoxia-ischemia in immature rat brain. *Stroke* **40**, 3107–3112 (2009).

69. Bidri, M. et al. Inhibition of mouse mast cell proliferation and proinflammatory mediator release by benzodiazepines. *Immunopharmacology* **43**, 75–86 (1999).

70. Xu, D. et al. Midazolam exposure impedes oligodendrocyte development via the translocator protein and impairs myelination in larval zebrafish. *Mol. Neurobiol.* **59**, 93–106 (2022).

71. Zhang, X. et al. Activated brain mast cells contribute to postoperative cognitive dysfunction by evoking microglia activation and neuronal apoptosis. *J. Neuroinflamm.* **13**, 127 (2016).

72. Chen, Y. Z. et al. Magnetic resonance imaging of glutamate in neuroinflammation. *Radiol. Infect. Dis.* **3**, 92–97 (2016).

73. Sall, J. W., Stratmann, G., Leong, J., Woodward, E. & Bickler, P. E. Propofol at clinically relevant concentrations increases neuronal differentiation but is not toxic to hippocampal neural precursor cells in vitro. *Anesthesiology* **117**, 1080–1090 (2012).

74. Paolicelli, R. C. et al. Microglia states and nomenclature: a field at its crossroads. *Neuron* **110**, 3458–3483 (2022).

75. Wittekindt, M. et al. Different methods for evaluating microglial activation using anti-ionized calcium-binding adaptor protein-1 immunohistochemistry in the cuprizone model. *Cells* **11**, 1723 (2022).

76. Qiao, H. et al. Propofol affects neurodegeneration and neurogenesis by regulation of autophagy via effects on intracellular calcium homeostasis. *Anesthesiology* **127**, 490–501 (2017).

77. Guo, S., Wang, H. & Yin, Y. Microglia polarization from M1 to M2 in neurodegenerative diseases. *Front. Aging Neurosci.* **14**, 815347 (2022).

78. Krishnan, M. L. et al. Integrative genomics of microglia implicates DLG4 (PSD95) in the white matter development of preterm infant. *Nat. Commun.* **8**, 428 (2017).

79. Kantamneni, S. Cross-talk and regulation between glutamate and GABAB receptors. *Front. Cell Neurosci.* **9**, 135 (2015).

80. Kotani, Y., Shimazawa, M., Yoshimura, S., Iwama, T. & Hara, H. The experimental and clinical pharmacology of propofol, an anesthetic agent with neuroprotective properties. *CNS Neurosci. Ther.* **14**, 95–106 (2008).

81. Wang, S. et al. The changing of α5-GABAA receptors expression and distribution participate in sevoflurane-induced learning and memory impairment in young mice. *CNS Neurosci. Ther.* **30**, e14716 (2024).

82. Zurek, A. A., Bridgwater, E. M. & Orser, B. A. Inhibition of α5 γ-aminobutyric acid type A receptors restores recognition memory after general anesthesia. *Anesth. Analg.* **114**, 845–855 (2012).

83. Zhang, S. et al. Cerebral mast cells contribute to postoperative cognitive dysfunction by promoting blood brain barrier disruption. *Behav. Brain Res.* **298**, 158–166 (2016).

84. Xu, F. et al. Prolonged anesthesia induces neuroinflammation and complement-mediated microglial synaptic elimination involved in

neurocognitive dysfunction and anxiety-like behaviors. *BMC Med.* **21**, 7 (2023).

85. Helmy, S. A. K. & Al-Attiyah, R. J. The immunomodulatory effects of prolonged intravenous infusion of propofol versus midazolam in critically ill surgical patients. *Anaesthesia* **56**, 4–8 (2001).

86. Ots, H. D., Tracz, J. A., Vinokuroff, K. E. & Musto, A. E. CD40–CD40L in neurological disease. *Int. J. Mol. Sci.* **23**, 4115 (2022).

87. Kim, D. Y., Jeoung, D. & Ro, J. Y. Signaling pathways in the activation of mast cells cocultured with astrocytes and colocalization of both cells in experimental allergic encephalomyelitis. *J. Immunol.* **185**, 273–283 (2010).

88. Kim, D. Y., Hong, G. U. & Ro, J. Y. Signal pathways in astrocytes activated by cross-talk between of astrocytes and mast cells through CD40-CD40L. *J. Neuroinflamm.* **8**, 25 (2011).

89. Suurmond, J. et al. Communication between human mast cells and CD4+ T cells through antigen-dependent interactions. *Eur. J. Immunol.* **43**, 1758–1768 (2013).

90. Ottum, P. A., Arellano, G., Reyes, L. I., Iruretagoyena, M. & Naves, R. Opposing roles of interferon-gamma on cells of the central nervous system in autoimmune neuroinflammation. *Front. Immunol.* **6**, 539 (2015).

91. Abellanas, M. A. et al. Midbrain microglia mediate a specific immunosuppressive response under inflammatory conditions. *J. Neuroinflamm.* **16**, 233 (2019).

92. Suurmond, J., Dorjée, A. L., Huizinga, T. W. J. & Toes, R. E. M. Human mast cells costimulate T cells through a CD28-independent interaction. *Eur. J. Immunol.* **46**, 1132–1141 (2016).

93. Zhou, X. Y., Chen, K. & Zhang, J. A. Mast cells as important regulators in the development of psoriasis. *Front. Immunol.* **13**, 1022986 (2022).

94. Ali, M. Y., Knight, D. & Howlader, M. M. R. Nonenzymatic electrochemical glutamate sensor using copper oxide nanomaterials and multiwall carbon nanotubes. *Biosens. (Basel)* **13**, 237 (2023).

95. Zeynaloo, E. et al. Design of a mediator-free, non-enzymatic electrochemical biosensor for glutamate detection. *Nanomedicine* **31**, 102305 (2021).

96. Soldatkina, O. V. et al. A novel amperometric glutamate biosensor based on glutamate oxidase adsorbed on silicalite. *Nanoscale Res. Lett.* **12**, 260 (2017).

97. Sun, Y. et al. In vivo glutamate sensing inside the mouse brain with perovskite nickelate–nafion heterostructures. *ACS Appl Mater. Interfaces* **12**, 24564–24574 (2020).

98. Ganesana, M., Trikantzopoulos, E., Maniar, Y., Lee, S. T. & Venton, B. J. Development of a novel micro biosensor for in vivo monitoring of glutamate release in the brain. *Biosens. Bioelectron.* **130**, 103–109 (2019).

99. Spitz, S., Schobesberger, S., Brandauer, K. & Ertl, P. Sensor-integrated brain-on-a-chip platforms: improving the predictive validity in neurodegenerative research. *Bioeng. Transl. Med.* **9,** e10604 (2023).

100. Akbari, S. et al. Robust, long-term culture of endoderm-derived hepatic organoids for disease modeling. *Stem Cell Rep.* **13**, 627–641 (2019).

101. Lancaster, M. A. & Knoblich, J. A. Generation of cerebral organoids from human pluripotent stem cells. *Nat. Protoc.* **9**, 2329–2340 (2014).

102. Ertürk, A. et al. Three-dimensional imaging of solvent-cleared organs using 3DISCO. *Nat. Protoc.* **7**, 1983–1995 (2012).

103. Cai, R. et al. Panoptic imaging of transparent mice reveals whole-body neuronal projections and skull–meninges connections. *Nat. Neurosci.* **22**, 317–327 (2019).

104. Cai, R. et al. Whole-mouse clearing and imaging at the cellular level with vDISCO. *Nat. Protoc.* **18**, 1197–1242 (2023).

105. Wu, T. et al. clusterProfiler 4.0: a universal enrichment tool for interpreting omics data. *Innovation* **2**, 100141 (2021).

Acknowledgements

Author contributions
P.S.M. and S.Y. equally contributed to this work. P.S.M., S.Y., J.M., M.N., and Y.C.O. designed the experiments, analyzed the data and wrote the paper. O.Y.C., E.Y., C.B.A., A.G., and A.E. wrote, reviewed and edited the paper. O.Y.C. conceived the project, supervised all the experiments and edited the whole paper. All authors have read and agreed to the published version of the manuscript.

Competing interests
The authors declare no competing interests.

Additional information
Supplementary information The online version contains supplementary material available at https://doi.org/10.1038/s42003-024-07313-z.

Correspondence and requests for materials should be addressed to Ozlem Yesil-Celiktas.

Peer review information *Communications Biology* thanks Jagdeep Sandhu and the other, anonymous, reviewer(s) for their contribution to the peer review of this work. Primary HAandling Editor: Christina Karlsson Rosenthal.

Reprints and permissions information is available at http://www.nature.com/reprints

Publisher's note Springer Nature remains neutral with regard to jurisdictional claims in published maps and institutional affiliations.